A competition–species model for water vapour-aerosol-cloud-rain interactions

Faustine Mascaut, Olivier Pujol, Jérôme Brioude, Andrew Jensen, Marc Lefranc, Stéphanie Evan, Suzanne Crumeyrolle

▶ **To cite this version:**

Faustine Mascaut, Olivier Pujol, Jérôme Brioude, Andrew Jensen, Marc Lefranc, et al.. A competition–species model for water vapour-aerosol-cloud-rain interactions. Atmospheric Research, 2023, Atmospheric Research, pp.106588. 10.1016/j.atmosres.2022.106588 . hal-04474587

HAL Id: hal-04474587
https://hal.univ-lille.fr/hal-04474587v1

Submitted on 8 Jan 2025

HAL is a multi-disciplinary open access archive for the deposit and dissemination of scientific research documents, whether they are published or not. The documents may come from teaching and research institutions in France or abroad, or from public or private research centers.

L'archive ouverte pluridisciplinaire **HAL**, est destinée au dépôt et à la diffusion de documents scientifiques de niveau recherche, publiés ou non, émanant des établissements d'enseignement et de recherche français ou étrangers, des laboratoires publics ou privés.

Distributed under a Creative Commons Attribution - NonCommercial 4.0 International License

Version of Record: https://www.sciencedirect.com/science/article/pii/S0169809522005749
Manuscript_2a65fc32cbe2b13572b12e5122be81c1

Atmospheric Research 284 (2023) 106588

Contents lists available at ScienceDirect

Atmospheric Research

journal homepage: www.elsevier.com/locate/atmosres

A competition–species model for water vapour-aerosol-cloud-rain interactions

Faustine Mascaut [a,*], Olivier Pujol [a,*], Jérôme Brioude [b], Andrew Jensen [c], Marc Lefranc [d], Stéphanie Evan [b], Suzanne Crumeyrolle [a]

[a] Université de Lille, CNRS, UMR 8518 - LOA - Laboratoire d'Optique Atmosphérique, F-59000 Lille, France
[b] Laboratoire de l'Atmosphère et des Cyclones (LACy), UMR 8105, Météo France/CNRS/Université de La Réunion, St Denis de La Réunion, France
[c] Mathematical Sciences, Northland College, Ashland 54806, WI, USA
[d] Université de Lille, CNRS, UMR 8523 - PhLAM - Physique des Lasers, Atomes et Molécules, 59655 Villeneuve d'Ascq, France

ARTICLE INFO

Keywords:
Water vapour
Aerosol-cloud-rain interactions
Species competition dynamics
Cloud physics
Cloud field organisation
Tropospheric measurements

ABSTRACT

In this paper, a non-linear bulk model inspired from species competition dynamics is proposed in order to describe the physics of water vapour-aerosol-cloud-rain interactions. Despite the complexity of such interactions, certain non-trivial aspects of the macro behavior of a cloud are predictable without concerning the full complexity of the dynamical system. The model is for warm clouds (no ice) and it consists in a set of three non-linear differential equations. This species-competition model is confronted with *in situ* measurements in different situations: for pristine environments (1) at the high-altitude Maïdo Observatory (Indian Ocean, Reunion Island) and (2) in a pure oceanic context around the Reunion Island (AEROMARINE field campaign) and for a continental urban context (3) in Lille (North of France). Compared with observations (radar, radiometric measurements), it is shown that, whatever the situation considered, the model reproduces efficiently the macro features of clouds, like cloud occurrences, cloud water content magnitudes, and cloud-rain links. The model is adapted to a two-dimensional (horizontal) grid and its predictions are compared with the ERA5 reanalyses above the Hauts-de-France region and in the pristine Southwest Indian Ocean (around Reunion Island). Furthermore, satellite data enable to corroborate that the model clearly shows promising results for the horizontal cloud field organization. The spatiotemporal resolution of this model is adaptable according to the needs and it can be used in any region and at the desired altitude provided that data be available for implementation. In this paper, it is also suggested that the model may be fruitful to derive from measurements, by means of an optimization scheme, different theoretical parameters not easy to determine. The model runs on a laptop with a relatively short time (of the order of the minute); it is not intended to supplant comprehensive models, but it may be fruitful to understand the essential mechanisms in warm cloud formation.

1. Introduction

Despite recent advances, atmospheric models incompletely capture the effects of aerosols on climate through their interactions with clouds (Rosenfeld et al., 2014). Indeed, these interactions are complex and require parameterizations for wide ranges of time (from the near-instantaneous Twomey effect to the longer timescales required for cloud adjustments - Gryspeerdt et al., 2021) and space scales (from microphysical processes to the organization of cloud fields - Stevens et al., 2020). However, the treatment of aerosols in these models is hampered by the lack of measurements and the still incomplete understanding of the mechanisms involving clouds. The modification of the Earth's radiative budget caused by aerosol-cloud interactions is still highly uncertain and these uncertainties (they are between -0.71 and -0.14 W m^{-2} with a 5–95% confidence range according to Bellouin et al., 2020) have been accentuated by anthropogenic aerosol emissions since the beginning of the industrial era (Bellouin et al., 2020).

The effect of aerosol-cloud interactions is not limited to radiative forcing. At the end of the "food chain" of aerosol-cloud processes, precipitation can be affected by aerosols. Thus, the interactions between aerosols, clouds and precipitation are intrinsically linked and must be treated as a unique problem when attempting to better understand such

* Corresponding authors.
E-mail addresses: faustine.mascaut@univ-lille.fr (F. Mascaut), olivier.pujol@univ-lille.fr (O. Pujol).

https://doi.org/10.1016/j.atmosres.2022.106588
Received 17 August 2022; Received in revised form 26 November 2022; Accepted 19 December 2022
Available online 23 December 2022
0169-8095/© 2022 Elsevier B.V. All rights reserved.

© 2022 published by Elsevier. This manuscript is made available under the CC BY NC user license
https://creativecommons.org/licenses/by-nc/4.0/

a complex system (Koren and Wang, 2008).

Aerosol-cloud interactions still need to be investigated with various approaches for better understanding and in order their representation in current climate models to be improved. The relation that aerosols and clouds have throughout the life cycle of a cloud (formation/dissipation, lifetime, spatiotemporal evolution, etc.) is still an active field of cloud physics research (Seinfeld et al., 2016); cloud field organization at the mesoscale is not well parameterized in numerous climate simulations (Bony et al., 2000). There are currently two main modeling approaches to climate theory: (1) to use general circulation models which try to represent, as exhaustively as possible, all of the complex dynamics (at different scales) of the atmosphere and/or ocean, and (2) to focus on idealized (*i.e.* simplified but physically realistic) models with the aim to understand the behavior of a specific phenomenon in the climate system. The models of the first kind require powerful computers and are time consuming whereas those of the second kind, by capturing the essential physics, can run quickly on a laptop. Held (2005) has underlined the gap in these two approaches and has highlighted the need to understand idealized nonlinear systems with only a few degrees of freedom before being able to understand the full complexity of the climate system. For this, it is interesting to use an interdisciplinary approach by reconciling physics, climate sciences and mathematics (Wettlaufer, 2016).

Following this point of view, and in order to understand the behavior and evolution of aerosol-cloud-rain interactions, Pujol and Jensen (2019) introduced a bulk model which follows the idea of modeling cloud–precipitation interaction through species competition that exhibits prey-predator behavior with rain as predator and cloud droplets as prey. In this model, a cloud is considered as a physical system defined by three populations (degrees of freedom): the cloud water content L_c (in g m^{-3}), the rain water content L_r (in g m^{-3}) and the concentration (in number) of cloud droplets N_d (in cm^{-3}). The values of the three macroscopic populations are unique, *i.e.* they concern the whole cloud (there is no spatial variation). The model is based on the following system of bulk coupled-first order differential equations:

$$\begin{cases} \dfrac{\mathrm{d}L_c}{\mathrm{d}t} = A_c L_c - K N_d^{-2} L_c^4 - k_r L_c L_r \\ \dfrac{\mathrm{d}L_r}{\mathrm{d}t} = -A_r L_r + K N_d^{-2} L_c^4 + k_r L_c L_r \\ \dfrac{\mathrm{d}N_d}{\mathrm{d}t} = A_c (N_0 - N_d) - k_c L_c^2 - k_r L_r N_d \end{cases} \tag{1}$$

Some macro-scale properties of cloud-precipitation interactions are highlighted using these three relatively simple equations of three degrees of freedom, rather than a fine-scale description with complete microphysical details. The meaning of the different terms of this system of equations and of the different constants involved, namely the set $\{A_c, A_r, K, k_r, k_c\}$ are summarized in Table 1. Pujol and Jensen (2019) have shown that the aerosol-cloud-rain system, as modeled by Eq. (1), exhibits realistic oscillating behaviors, especially a delay between cloud formation and rain appearance of a few tens minutes (≈20–30 min). We recall that in this last reference, as here in this paper, the kinetic constants have *net* values representing an equilibrium. In particular, the net value of A_c represents a balance between evaporation and condensation.[1]

A precision is in order at this stage. As detailed in Pujol and Jensen (2019), the terms in Eq. (1) are a straightforward consequence of the stochastic collection equation (SCE) with polynomial kernel, as explained in Seifert and Beheng (2001). The SCE results from collision theory and involves realistic size spectra (many often, gamma distributions). Details on the SCE can also be found in Pruppacher and Klett (2010). Note also that N_d and L_c are two independent degrees of freedom (double-scheme), which means that, in the simulations, an increase (decrease) of N_d concomitant to a decrease (increase) of L_c, can be reasonably interpreted as a creation of big (small) droplets.

In the life cycle of clouds and precipitation, not only cloud condensation nuclei (CCN) are important but water vapour is also a key element. This is because cloud droplets form in the presence of CCN on which water vapour can condense. According to the latest assessments (Douville et al., 2021, Fig. 8.1), the water vapour flux from the surface towards the troposphere is about 540 km^3/yr with an oceanic contribution of about 86%, corresponding to approximately six times that of land (accuracy of 10%). All of this water vapour is transformed into precipitation. A metaphor helps to understand the role of water vapour and aerosol in cloud formation. Let us imagine a cloud as motor engine where water vapour is the fuel and the aerosol the spark plug. No matter how many spark plugs (aerosols) there are, the engine (a cloud) will not ignite or go faster if it runs out of fuel (water vapour); it will eventually stop. That is to say that, in an air mass, the liquid water content cannot increase with no water vapour available; it can only decrease. Cloud life (birth, growth, death) is a subtle interplay between water vapour and aerosols. Water vapour has also an impact on aerosol optical properties: *e.g.* Zhu et al. (2019) reported, from AERONET measurements in China, that

Table 1
Details (physical processes represented, values and units) of the different parameters in Eq. (1) (Pujol and Jensen, 2019).

Variables	Physical meaning	SI units
L_c	Cloud water content	g m^{-3}
L_r	Rain water content	g m^{-3}
N_d	Cloud droplet number concentration	cm^{-3}
N_0	Background aerosol concentration	cm^{-3}
Kinetic constants	Physical meaning	Value/SI units
A_c	Positive constant which gives the timescale ($\tau_c = 1/A_c \simeq 50$ min) of cloud water content evolution	0.02 min^{-1}
A_r	Positive constant which gives the timescale ($\tau_r = 1/\lvert A_r\rvert \simeq 10$ min) of rain water content evolution (rain out process)	0.1 min^{-1}
k_c	Constant from the cloud water kernel (Seifert and Beheng, 2001)	7.55×10^{11} cm^{3}g^{-2} min^{-1}
k_r	Constant from the rain water kernel (Seifert and Beheng, 2001)	3.47×10^{5} cm^{3}g^{-2} min^{-1}
K	$K = [k_c/(20x^\star)](\nu+2)(\nu+4)(\nu+1)^{-2}$ where $x^\star$ is a cloud drop mass separating droplets from raindrops (precisely, $x^\star = L_r/N_r$, where N_r is the raindrop number concentration), and $\nu = 2$ is the shape parameter of the gamma distribution (Long, 1974)	3.41×10^{17} cm^{3}g^{-3} min^{-1}
Terms of Eq. (1)	Physical meaning	SI units
$A_c L_c$	Sources of cloud water content	g m^{-3} min^{-1}
$-A_r L_r$	Sinks of rain water content	g m^{-3} min^{-1}
$K N_d^{-2} L_c^4$	Autoconversion: a key microphysical process whereby raindrops are formed by collision-coalescence processes of cloud droplets.	g cm^{-3} m^{-7} min^{-1}
$k_r L_r L_c$	Accretion of cloud water by rain water	cm^{3}m^{-6} min^{-1}
$A_c(N_0 - N_d)$	Supply of cloud droplets from the surroundings	cm^{-3} min^{-1}
$-k_c L_c^2$	Cloud droplet self-collection	cm^{-3} min^{-1}
$-k_r L_r N_d$	Accretion of cloud water by rain water	g m^{-3} min^{-1}

[1] The evaporation process would consist in a term of the form $-A_1 L_c$ with $A_1 > 0$, while condensation is $A_2 L_c$ with $A_2 > 0$. The net process is $(A_2 - A_1)L_c$, *i.e.*$A_c L_c$. Choosing $A_c > 0$ is obvious: if A_c were negative, the model would never form clouds. This is completely analogous to a chemical reaction: $A + B \leftrightarrow C$ is an equilibrium characterized by a kinetic constant being the balance between the competing direct and inverse reactions.

an increase of the column of water vapour by 0.1 cm could enhance the aerosol direct radiative forcing at the bottom of the atmosphere by about 1.1–2.8 W m^{-2}. Furthermore, Stathopoulos et al. (2021) has shown causal relationships between water vapour and *AOD*s, cloud cover, and cloud optical thickness. It is generally recognized that the understanding of the effects of aerosols on cloud formation and life cycle needs improvement. We hypothesize that a way to achieve a better understanding is to consider water vapour explicitly in the model as an independent variable, as supported by the latest IPCC report (Douville et al., 2021). Indeed, high-resolution models show that aerosol concentrations can have a significant impact on ambient humidity and therefore on cloud formation. In addition, our study takes place in an oceanic context, dominated by marine aerosols. These aerosols are mostly hygroscopic particles whose optical properties vary according to atmospheric humidity. Thus, adding this parameter would make it possible to study the sensitivity of marine aerosols to humidity.

This is why, in this paper, the previous model of Pujol and Jensen (2019) is generalized by introducing explicitly the water vapour content (L_v) as a new variable in the system of equations. Doing so, a model of water vapour-aerosol-cloud-rain dynamics is presented in this paper. To our knowledge there is not such an explicit effect in the current cloud models. Furthermore, an estimate of the Cloud Optical Thickness (COT) and of the cloud albedo (R_c) is proposed. The system of three equations which describes the new model is presented in the next section. This system is used in three real situations, *i.e.* with experimental data, which are characterized by different aerosol and water vapour contents. These situations are:

- In Saint Denis (Reunion Island) in the Indian Ocean which is a pristine region (where land and human activities have few impacts, Mallet et al., 2018), in a background aerosol environment which can be considered close to pre-industrial conditions. This case study allows us to evaluate the behavior of aerosol-cloud-rain interactions under clean marine conditions, with little or no anthropogenic contributions. It is worth recalling that oceans cover about 70% of the Earth surface and are thus of prime importance in the climate system. Especially, they represent the most important exchanges with the low troposphere of energy and humidity and they are a reserve of CCN.
- At the Maïdo Observatory (Reunion Island, 21.1°S, 55.4°E), at an altitude of 2.2 km above sea level, in the same pristine conditions as before (Baray et al., 2013). The specificity of this site (presented in detail later) is its own context and altitude.
- In an urban/continental context in Lille (North of France). This case study makes it possible to evaluate the impact of human contributions on aerosol-cloud-rain interactions.

These three case studies are detailed in Section 2.2. They assess aerosol-water vapour-cloud-rain interactions under pristine conditions (*i.e.* with little or no anthropogenic contributions) and in a continental urban region where anthropogenic contributions to aerosol concentrations are in the majority. The associated experimental data are *in situ* measurements from the AEROMARINE field campaign in Saint Denis (Reunion Island; Mascaut et al., 2022), those from the Maïdo Observatory (Reunion Island) as well as measurements made on the ATmospheric Observations in liLLe (ATOLL[2]) platform in Lille (all presented in Section 2.2).

To assess the realism of this model, the results are compared with radiometric and radar measurements in Section 3. Finally, in order to evaluate the horizontal organization of cloud fields, the model is transposed to a two-dimensional (2D) horizontal grid above the Indian Ocean and the Hauts-de-France region (centred around Lille) and compared with ERA5 reanalyses and satellite observations (Section 3.4).

A conclusion and some perspectives are given in Section 4.

2. Description of the species-competition model with water vapour

2.1. Model operation

As already indicated above, water vapour is of fundamental importance for the understanding of aerosol-cloud-rain interactions. Consequently, the initial equations (Eq. (1), from Pujol and Jensen, 2019), are modified by introducing water vapour as an *explicit* variable.

The new model is defined by the following set of equations:

$$\begin{cases} \dfrac{dL_c}{dt} = \alpha A_c (L_v - L_c) - K N_d^{-2} L_c^4 - k_r L_c L_r \\ \dfrac{dL_r}{dt} = -A_r L_r + K N_d^{-2} L_c^4 + k_r L_c L_r \\ \dfrac{dN_d}{dt} = A_c^{'} (L_v - L_c)(N_0 - N_d) - k_c L_c^2 - k_r L_r N_d \end{cases} \quad (2)$$

where L_c, N_d and L_r have the meaning already indicated above, and where L_v is the water vapour content (in g m^{-3}). This quantity is not constant; rather its temporal variation cannot be neglected as measurements reveal (air mass absolute humidity evolve quickly, see Section 2.2 and further in the text). Compared to Eq. (1), the change is the term which represents the supply of cloud droplets by condensation. Clearly, from this process alone, the mass of cloud water cannot exceed the mass of water vapour, so L_c must be lower than L_v. If, at time t, L_c reaches L_v (saturation), then $L_v(t) - L_c(t) = 0$ g m^{-3} (condensation does not occur any more). Condensation can occur, at a later time, if $L_v - L_c$ becomes positive. It is worth mentioning that the term $A_c(L_v - L_c)$ is analogous to that which represents the behaviour of a capacitor connected to a generator: the electrical charge (here L_c) cannot be greater than the electrical charge (here L_v) that the generator can furnish. The term $A_c^{'}(L_v - L_c)(N_0 - N_d)$ can be envisioned as $A_{c,v}(N_0 - N_d)$ where $A_{c,v}$ is a kinetic constant which depends upon the water vapour content. Indeed, the higher the L_v, the higher $A_{c,v}$ and the shorter the timescale to form a droplet.

The factor α is a binary parameter which can be equal to 0 or 1, depending on a relative humidity threshold (typical of the studied area). Such a threshold is a computational boolean to avoid models generating clouds when humidity conditions are not favorable. The threshold is taken below 100% in order to take into account that thermodynamical fluctuations can (super) saturate an air mass and also possible dynamical features, like air mass lifting, propitious to cloud formation. In other words, this threshold indicates to the computer that it must stop to condense water vapour if *RH* is not high enough. Here, we will use a threshold of 70% or 80% depending on the concrete situation investigated. The value 70% is for the Maïdo site because of the presence of orographic winds which lift moist air and favour cloud formation. These values are typically those encounter in models (*e.g.* RAMS, WRF, Meso-NH). Hence, if $RH(t) > 70\%$ (or $RH(t) > 80\%$), then $\alpha = 1$, otherwise $\alpha = 0$. The value of the *RH* threshold is based on (independent) measurements, according to the situation considered, precisely the correspondence between *RH* values and the presence of clouds. This makes the chosen values representative of the situations. Fortunately, some tests have indicated that our model is not a lot sensitive to the *RH* threshold at more or less than 5%. However, if the threshold were too low, the model would generates clouds which rarely (to not say never) dissipate (for the model, there is always enough humidity to give a cloud). Conversely, if the threshold were too high, clouds never form, (the model "understands" that there is humidity is never sufficient).

This new set of equations (Eq. (2)) can be formulated differently by defining the following quantities, at time t:

[2] https://www-loa.univ-lille1.fr/observations/plateformes.html?p=lille#.

- $L_{c,d} = L_v - L_c$ is the cloud water content *potentially available*, *i.e.* if water vapour condenses.
- $N_a = N_0 - N_d$ is the concentration (in number) of CCN in the system under the assumption that one droplet formed corresponds to one dissolved, or wet, aerosol. Otherwise stated, N_a is the number of dry aerosol able to condense water vapour.
- $L_l = L_r + L_c$ is the quantity of liquid water in the system.

The SI units of $L_{c,d}$ and L_l are obviously those of L_c (or L_r), and that of N_a is that of N_d (or N_0). These three quantities constitute an alternative to the four above variables which gives another insight.

Using these three variables, the system of Eq. (2) can be written as follows:

$$\begin{cases} \dfrac{dL_{c,d}}{dt} = \dfrac{dL_v}{dt} - \alpha A_c L_{c,d} + K(N_0 - N_a)^{-2}(L_v - L_{c,d})^4 + k_r(L_v - L_{c,d})(L_l + L_{c,d} - L_v) \\ \dfrac{dL_l}{dt} = \alpha A_c L_{c,d} - A_r(L_l + L_{c,d} - L_v) \\ \dfrac{dN_a}{dt} = \dfrac{dN_0}{dt} - A_c' L_{c,d} N_a + k_c(L_v - L_{c,d})^2 - k_r(L_l + L_{c,d} - L_v)(N_a - N_0) \end{cases} \quad (3)$$

From $L_c(t)$ and $N_d(t)$ given by Eq. (2), one can calculate the quantity $\beta = [9\pi N_d L_c^2/(2\rho_w^2)]^{1/3}$ which enters into the definition of the cloud optical thickness: $COT \propto h\beta$ (Seinfeld and Pandis, 1998) where h is the cloud thickness and $\rho_w = 1000\,\mathrm{kg\,m^{-3}}$ the liquid water density. Because our model (Eq. 2) does not provide any information about h, a solution may be to focus only on β and to consider a *COT* for a cloud of thickness unity. Another possibility is to estimate h, either using a realistic statistical value or using experimental data. It is this last option which has been chosen in this work. To estimate h at each time step, we have used the liquid water profiles measured by a microwave radiometer (presented hereafter). An evaluation of the cloud albedo R_c of the simulated cloud can be evaluated using $R_c = COT/(COT+7.7)$ (Seinfeld and Pandis, 1998). Clouds with more droplets are brighter (at constant liquid water path), and therefore they reflect more short-wave radiation back into space, exerting negative radiative forcing. This is the radiative forcing of aerosol-cloud interactions (RFaci), also called the first indirect effect or cloud albedo effect, *e.g.* Douville et al. (2021).

2.2. Input data to feed model

To run the model, the evolution of three input parameters is needed: $N_0(t)$, $L_v(t)$, and $RH(t)$ for the determination of α. Another input is the cloud thickness h, which is needed for the calculation of the *COT* of the simulated clouds.

As indicated in the introduction, three different sets of observations have been used: (1) maritime/mountainous (Maïdo Observatory, Reunion Island), (2) oceanic (Saint-Denis, Reunion Island); and (3) urban (Lille, ATOLL station). Below is a short description of these three sites. For all of them, L_v, N_0, RH and h are provided by the following instruments.[3]

- A MicroWave Radiometric Profiler (MWRP, RPG-HATPRO G5), which continuously (time resolution 1 min) measures thermodynamic vertical profiles (0–10 km)[4] of the tropospheric absolute and relative humidities. Such an instrument has already been proved to be of considerable interest to investigate processes triggered by water vapour (*e.g.* Louf et al., 2015). The MWRP is also able to provide vertical profiles of the liquid water content (LWC), which is then used to estimate h: in the presence of a cloud ($LWC \neq 0\ \mathrm{g\,m^{-3}}$), the difference between the maximum and minimum altitudes for which $LWC \neq 0\ \mathrm{g\,m^{-3}}$ are assumed to coincide with h. It has to be noted that the LWC given by the MWRP is an approximate value derived from its upper limit (*i.e.* the adiabatic LWC) using the empirical relation of Karstens et al. (1994). We precise that multi-layer clouds have been excluded, so that the h derived is for one cloud. There are two reasons for this: (1) radiometric observations have shown very few cases of multi-layer clouds for the examples considered here; (2) focus is put on liquid low-level clouds. In the very few probable presence of a, *e.g.*, two-layer clouds, there would be two altitude intervals for which $LWC \neq 0$, but one can just consider the cloud of lowest altitude, assuming inter-layers independence. In terms of the bulk model presented in this manuscript, dealing precisely with multi-layer clouds would require at least two values of h and as many systems of equations (not necessarily uncoupled, since contiguous layer may interact) as cloud layers.
- A Condensable Particle Counter (CPC) TSI (model 3007 during AEROMARINE and model 3776 at the Maïdo Observatory), which provides the concentrations (in number) of aerosols with sizes larger than 10 nm, *viz.* in the Aïtken, accumulation and coarse modes. The relative accuracy is $\pm$ *20%*. In order to avoid underestimating N_0, and therefore its impact on cloud formation, it is important to consider the full range of sizes available, even the smallest aerosol size. Indeed,Xu et al. (2022)have shown that the contribution of Sea Salt Aerosols (SSA) to the global CCN number, in particular the SSA in the Aïtken mode (size larger than *10 nm*), has been neglected in the literature. Their study has highlighted that *SSA* are present in all size ranges and that, therefore, the number of *CCN* is particularly underestimated in regions of strong winds. It is thus reasonable to identify N_0 with the CCN number. This is not a severe assumption, since Mascaut et al. (2022) have showed that, in this marine context (Reunion Island), aerosol sizes is 132 nm on average, which is a typical order of magnitude for CCN, and Mallet et al. (2018) showed that more than 80% these aerosols are SSA. The ionic properties of such aerosols is propitious to cloud droplet formation.

In the case of the ATOLL station, the CPC is the TSI model 3775 (relative accuracy of $\pm$10%). It was, in particular, associated, inside a SMPS (Scanning Mobility Particle Sizer), with a differential mobility analyzer (Villani et al., 2007) which previously (*i.e.* before counting) selected particles according to their size from 15.7 nm up to 800 nm. In Lille, assuming that N_0 is the number of CCN may appear not obvious. But, in the equation of the model N_0 can be changed the CCN number (if measurable) or, formally, by βN_0, with $0 \leqslant \beta \leqslant 1$ (*i.e.*N_0 is decreased). We will come back to this timely. Also, we will see later (Section 2.3) that a way to deal with such "uncertainties", which finally reflect the specificity of a region, can be addressed by modifying the set of kinetic constants, *viz.* optimizing it to the region.

Moreover, we have to assume that ground-based measurements represent, or at least are close to, the aerosol concentrations at the altitude of cloud formation, because we do not have the possibility to access the latter, to the exception of AEROMARINE where airborne measurements were realized (see Mascaut et al., 2022). The assumption is not problematic: N_0 can be weighted by β (this time not necessarily lower than 1), if the information is known, and as just mentioned above optimizing of the constants is helpful to circumvent the problem of no exact colocalization between the system and the measures.

Note that L_v and N_0, as being measured, are not only resulting from local (algebraic) production but also from external transport.

[3] Data used in this paper are assumed to be reliable for two reasons: (1) some come from Mascaut et al. (2022) and the co-authors of this reference who are PI of the instruments involved have checked, controlled and validated measurements; (2) Maïdo and ATOLL are long-life platforms with engineers and technical staff controlling regularly data quality. Data are available on https://ebas-data.nilu.no/Default.aspx (Maïdo Observatory) and on https://loa.univ-lille.fr/observations/plateformes.html?p=lille(ATOLL); they can be furnished by e-mailing the corresponding author of the present paper.

[4] The origin of the altitude for these profiles is the position of the instrument.

2.2.1. Maïdo Observatory (Reunion Island)

The Observatory is in a background of aerosols typical of a pristine environment under prevailing southeasterly trade winds in the marine boundary layer. The meteorological field in this region is characterized by wet (from November to April) and dry seasons (from May to October; Simu et al., 2021). The instruments based at the Maïdo Observatory enable long-term observations of the marine boundary layer (daytime) and of the free troposphere (night-time) (Guilpart et al., 2017; Foucart et al., 2018). In this study, we have analyzed the wet season using measurements made in February 2019.

The measured aerosol concentrations and humidity 1 km above the instrument, which have been introduced in our model with a time step of $\Delta t = 1$ min, are displayed on Fig. 1A. It can be seen that aerosol concentrations are low during night-time ($N_0 \leqslant 1000$ cm^{-3}) when the Observatory is located in the free troposphere. During daytime, under the influence of the marine boundary layer, N_0 can reach several thousands (*e.g.* two peaks at 5 000 and 10 000 cm^{-3}). The same behaviour can be observed for humidity: during night-time, $RH \leqslant 40\%$ and $L_v \leqslant 2$ g m^{-3} (approximately); during daytime RH is clearly greater than 40% and can peak at almost 90%. The water vapour content L_v is always greater than 2 g m^{-3}: it is rather close to 4 or 5 g m^{-3} with a peak at 8 g m^{-3} when $RH \approx 90\%$. The Maïdo offers thus situations with well marked nocturnal/diurnal differences characterized by relatively low (high) values of N_0, L_v and RH during night-time (daytime). This is related to a complex interplay between sea-land breezes, katabatic winds and a complex topography: air masses at the Maïdo Observatory have various origins (*i.e.* oceanic, from the vegetation present on the slopes of the Maïdo or from local human activities). Aerosols measured have thus various physico-chemical properties and thermodynamic parameters are quite variable.

2.2.2. Saint Denis (Reunion Island)

In this case, we have used *in situ* measurements from the AEROMARINE field campaign. This campaign, which took place in 2019 off the coast of Reunion Island, in a pristine environment considered to be close to pre-industrial conditions, allows the determination of the distribution of (marine) aerosols, to quantify a background concentration of natural aerosols and to characterize the aerosols in this context (Mascaut et al., 2022). It also gave the thermodynamical profiles of the troposphere (up to 10 km), especially humidity.

Fig. 1B displays $N_0(t), L_v(t)$ and $RH(t)$ in this context. It can be seen that L_v varies between 7 g m^{-3} and 10 g m^{-3}, and RH between 75% and 85%. Their evolution is rather stable with no significant variation on average. Similarly, N_0 is between 100 cm^{-3} and 500 cm^{-3}. These values are much lower than those measured at the Maïdo Observatory. This may be explained by in-flight concentrations measured in the free troposphere during the campaign, which are mainly of marine origin, whereas at the Observatory, aerosols of different origins are measured.

2.2.3. Urban context: Lille

The model is also fed with *in situ* measurements made in an urban environment. The data from the ATOLL platform in Lille (Hauts-de-France, France) provide a good example of such an environment. Lille is situated in the Hauts-de-France Region, which is a territory with little pronounced relief endowed with highly urbanized, industrialized but also rural areas. It is at the crossroads of atmospheric air masses enriched

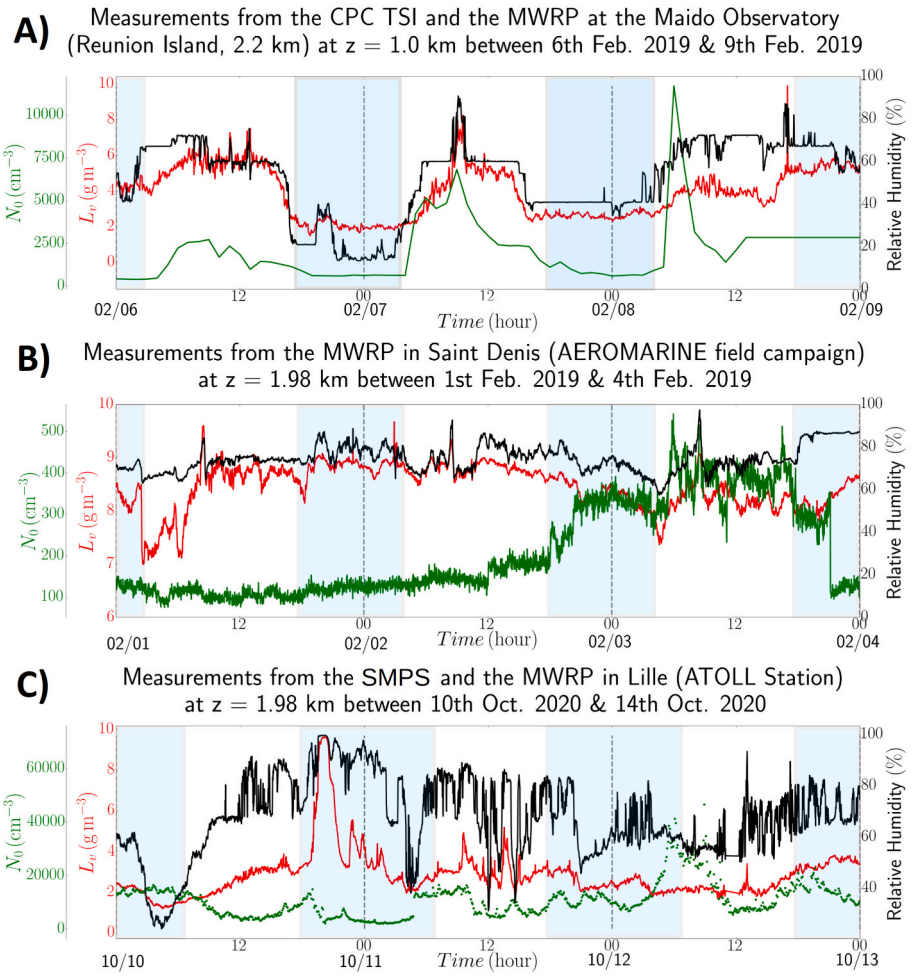

Fig. 1. Evolution of L_v (in g m^{-3}), RH (in %) and N_0 (in cm^{-3}) for three different situations: A) Maïdo Observatory, between 6th and 9th February 2019; B) Saint-Denis (Reunion Island), during the AEROMARINE field campaign, between 1st and 4th February 2019, and C) ATOLL station (Univ. Lille), from 10th to 14th October 2020. The data of humidity come from the MWRP, RPG-HATPRO G5 and the aerosol concentration are given by CPC TSI. The blue zones in the subfigures correspond to night-time measurements.

with gaseous and particulate elements (natural and anthropogenic), from sometimes very distant regions (Bovchaliuk et al., 2016; Chen et al., 2000; Laj et al., 2020; Mortier et al., 2013). The ATOLL station allows to monitor and investigate the aerosol-cloud-gas composition, and its evolution in the troposphere of the extreme north of France from the ground up to 10 km of height.

Fig. 1C shows an example of measures from ATOLL. It can be observed that $N_0 \approx 2 \times 10^4\ \mathrm{cm}^{-3}$ (on average), with a peak at about $4 \times 10^4\ \mathrm{cm}^{-3}$, which is much higher than in the Indian Ocean (pristine conditions). In addition, L_v in Lille (mid-latitude) is, on the whole, lower around 3 g m^{-3} than under the Tropical area of Reunion Island. One can note, however, that L_v can exceed 5 g m^{-3} and peak up to 10 g m^{-3} for some special events.

These three environments are thus interesting for a model of cloud formation, due to the different behaviours they represent in terms of humidity and aerosol concentration: well-marked diurnal/nocturnal separation (Maïdo case), relatively stable conditions with low values of N_0 and high values of L_v (Saint-Denis case), and rapidly changing N_0 and L_v evolutions (urban context in Lille).

2.3. Optimization of the kinetic constants

The model (Eq. (2)) uses a set of kinetic constants whose values presented in Table 1 permit to form clouds with realistic macroscopic features, like the order of magnitude and evolution of the cloud water and rain contents (L_c, L_r) (not shown). See Pujol and Jensen (2019) for some examples and details about these kinetic constants which come from collision theory and empirical considerations. These constants play a similar role as those used to characterize the kinetic and the efficiency of a chemical reaction. They belong to the larger class of reaction-rate theories (Hänggi et al., 1990).

Nonetheless, in order to improve the performance of the model the kinetic constants $\{K, k_r, k_c, A_c, A_c^{'}, A_r\}$ can be adapted to the region under consideration. In this way the best combination of kinetic constants can be obtained to reproduce the evolution of *in situ* measurements. The adjustment method consists in using a least square minimization technique. The procedure we have developed is as follows: (1) first, for each kinetic constant, we define an interval of physically possible values. Each interval contains a sufficient number of values, one of them being the "initial" value given in Table 1. From this, one thus defines a large number of independent sets of the kinetic constants. (2) We then perform N random draws in each interval. It means that for one draw, we have a set of six random values. After N draws, we have an ensemble of N independent sets of six values of the kinetic constants. (3) Each set is introduced in the model which runs for some time. We run the model N times with the same initial conditions, but with different set of values of the kinetic constants. (4) For a given run, at each time, we compare the modeled cloud water content, $L_c^{(mod)}(t)$, with the available measured cloud water content, $L_c^{(obs)}(t)$, and we define the score:

$$S(n) = \frac{1}{t_f} \sum_{t_i}^{t_f} \left[L_c^{(mod)}(t) - L_c^{(obs)}(t) \right]^2 \tag{4}$$

where t_i is the initial time of the simulation $(t_i = 0)$ and t_f is the final time. The above equation defines a function of n which is the number of a random draw $(1 \leqslant n \leqslant N)$: it gives the score S for the random draw numbered n. (5) The draw number n for which S is minimum is finally identified and the corresponding set of values of the kinetic constants is chosen. It is assumed that these values represent the best combination for cloud formation in the given environment (maritime, continental, etc) and the season under consideration. In the present work, $N = 5\,000$ and $t_f = 72$ h. Table 2 summarizes the results for the three situations presented in Section 2.2. The first column lists the constants with their SI units, the two next columns indicate the interval chosen and the fourth column is the number of values in this interval for the corresponding constant. The three columns on the right-hand side of the table give the optimized values of the constants.

Some comments are required. Here, $t_f = 72$ h, but of course the model can be run for shorter or longer times. That depends on the availability of measurements, on the macroscopic timescales wished for the life of the modeled clouds (hour, day, week, etc.) and whether S changes significantly, for a given value of N, as the simulation is running. In the three situations considered here, a final time of 72 h, was sufficient. Also, the number N should be high enough in order to have a large statistical ensemble of N random sets of the kinetic constants. Here, we have noticed that such sets did not change significantly after $N \approx 2\,000$. However, we have taken $N = 5\,000$ for better convergence. A similar comment can be made about the number of values for each kinetic constant in the range of values initially defined (about 10 millions). It is important to cover a large spectrum of values with a sufficient density of values. Our choice has been that given in Table 2. We assumed that L_c was the most suitable variable to use for calculating S to determine the best choice of kinetic constants. This assumption has been guided by three considerations: (1) L_c is the most important variable to characterize cloud formation, (2) L_c was the most reliable measurement available at any time (from monitoring of the MWRP) and, (3) L_c belongs to system of coupled equations, so that it reflects the behaviour of all the system, *viz.* the adjustmentof the kinetic constants, explicitly conducted with L_c, is also (implicitly) influenced by the two other degrees of freedom L_r and N_d. In principle, parameter identification could have been carried out with more sophisticated optimization techniques, such as those provided by genetic algorithms. However, the fact that running more than 5 000random draws improved adjustment very little, as we observed with up to 20 000draws, convinced us that the simple approach followed here was sufficient for our purposes.

The interest of adjusting kinetic constants is threefold.

- These constants have a theoretical origin to which empirical considerations are added. In general, the kinetic constants are not available (at least not directly, nor even in a relatively easy way) from measurements. The fact that different adjusted constants have been obtained in different meteorological situations suggests that the system of Eq. (2) could be used, not only as a model for cloud formation under given situations, but also as a tool to determine optimized values for the kinetic constants from observations in determined context. The potentiality of such an approach will be deepened in future work.
- In relation to this, the second advantage of optimization, by means of many independent observations, is that it allows to embrace efficiently the essential and inherent characteristics of the region of interest in terms of cloud formation. Indeed, this way, the mathematical space of the physical states (thermodynamics, dynamics, chemistry, orography, etc.) of the region is explored as much as possible. Consequently, favourable, and less favourable, conditions (whatever they are) for cloud formation are considered and "merged" statistically in a set of optimized constants. Hence, the latter contain the region specificities, in terms of aerosols properties, "local" (thermo) dynamics, geography (or topography). In the present paper, we put focus on the pristine Indian Ocean and Lille for the easy availability of a lot of data and for pristine oceans are our current scientific concern. But other regions could be tackled: provided that a lot of observations be available, constant can be readily optimized and the model used accordingly. As an interesting case would be the Arabian Peninsula, which is dry, rich in rather hydrophobic aerosols (dust and polluted aerosols with a marine component), sometimes under southeasterly and northwesterly wind influences, and where clouds can form (Weston et al., 2021; Yousef et al., 2020; Francis et al., 2021).
- The constant adjustment can be likened to technology using machine learning and Artificial Intelligence (AI). This new field of technology refers to the possibility for a machine to learn, to perceive its

Table 2
Kinetic constants calculated by a least square minimization method (see text for details) using observations in the three case studies.

				Observation sites		
Constant (SI unit)	Minimum value	Maximum value	Number of values	Maïdo observatory (Reunion Island)	AEROMARINE campaign (Saint Denis)	Lille (ATOLL station)
K ($cm^3g^{-3}min^{-1}$)	2.35×10^{18}	2.35×10^{20}	562	2.46×10^{18}	2.32×10^{18}	1.55×10^{18}
k_r ($cm^3g^{-2}min^{-1}$)	1.47×10^{4}	1.47×10^{6}	147	1.3×10^{6}	1.2×10^{6}	1.3×10^{6}
k_c ($cm^3g^{-2}min^{-1}$)	7.55×10^{10}	7.55×10^{12}	562	6.4×10^{12}	6.0×10^{12}	4.0×10^{12}
A_c (min^{-1})	0.0167	0.167	10	0.024	0.0185	0.0185
A_r (min^{-1})	0.0167	0.167	10	0.083	0.0167	0.0167
$A_c^{'}$ (min^{-1})	6.4×10^{4}	6.4×10^{5}	10	9.2×10^{4}	7.1×10^{4}	7.1×10^{4}

environment, manage these perceptions, solve problems, and take actions to achieve a specific goal. The computer machine receives data (already prepared or collected *via* sensors), analyzes them and reacts. By analogy, in our case, the data received by the system are the true state of the atmosphere (measurements from the MWRP and particle counters). The kinetic constants drawn randomly are the parameters which allow the model to adapt its behavior in order to get as close as possible to observations. This analogy is not the topic of this paper, but it seems to us interesting to mention that such features could be deepened and developed with the aim to adapt our model to such promising technology.[5]

3. Results

To get started, we take the following initial conditions for all of the case studies considered: $L_c(0) = 10^{-4}$ g m^{-3}, $L_r(0) = 10^{-4}$ g m^{-3} and $N_d(0) = 100$ cm^{-3}. The small values of $L_c(0)$ and $L_r(0)$ are chosen to eliminate potential numerical instabilities when choosing $L_c(0) = L_r(0) = 0$ g m^{-3}. The simulation time has been chosen to 72 h. The kinetic constants for each of these three observation sites are those obtained in the above section (Table 2).

3.1. Comparison with radar measurements

For the case study at the Maïdo Observatory, the measured L_v and N_0 presented in the previous section have been introduced in the model as input data for a simulation over 72 h between the 6th February 2019 (00:00 UTC) and the 8th February 2019 (23:59 UTC). Based on independent observations, a relative humidity threshold of 70% has been chosen for the determination of α.

Fig. 2 represents the evolution of the simulated L_v, L_c, L_r and N_d (top graph), with a zoom between 5 and 10 h after the initial time (middle graph), and the evolution of $L_{c,d}, L_l$ and N_a (bottom graph).

It can be seen that N_d evolves similarly to the background concentration of aerosols N_0 with values ranging, overall, between around 500 and 4000 cm^{-3}, except a peak at 12000 cm^{-3}. In addition, it appears clearly throughout the simulation that cloud formation (L_c peaks) is directly related to the evolution of the water vapour content (L_v), *viz.* clouds form when the absolute humidity is maximum or increasing.$L_c$is relatively small ($\lesssim$0.3 g m^{-3}) with three peaks exceeding 1 g m^{-3}. It is also observed that the formation of a cloud is followed, after about *10* or *20 min*, by the appearance of rain, which is a realistic cloud-rain behavior (rain forms generally after some tens minutes in a warm cloud; *e.g.*Rogers and Yau, 1996). Rain water content $L_r$can reach a maximum of 2 g m^{-3}. The variables L_l and N_a follow analogous behaviors to those of L_r and N_d, respectively. It is interesting to note, in particular, that N_a decreases when $L_c$increases, *i.e.* clouds consume aerosol in the system, and vice versa.

[5] These technologies are already common in remote sensing. For instance, the MWRP uses a neural network (suitable to the region where it is deployed) with around 26000 thermodynamical and dynamical profiles to further provide realistic and reliable measurements.

The simulated cloud water content L_c, can be compared with that derived from independent radar reflectivity measurements, at the same date, by the METEK MIRA-36 scanning Doppler cloud radar which was deployed at the Maïdo Observatory during the CONCIRTO ANR project. Focus has been put on measurements made vertically at an altitude of 1 km above the instrument. To make the comparison possible, the radar reflectivities (Z) have been converted into cloud water content by means of the Sauvageot formula (Sauvageot, 1992, p. 121-122), $Z = 6.8 \times 10^{-2} L_c^{1.9}$. This relation has empirical basis since it results from the interpolation of aircraft measurements (see also Sauvageot and Omar, 1987). Radar measurements are know to be suitable for cloud measurements and, in addition, no L_c data were available from the MWRP (at the Maïdo Observatory). For this site, the MWRP provides just humidity (L_v and RH) vertical profiles.

Cloud droplets correspond to radar reflectivities lower than −15 dBZ (Sauvageot and Omar, 1987). Fig. 3 displays the modeled and the radar-derived cloud water contents. It can be seen that, on the overall, the model reproduces well the orders of magnitude of $L_c (L_c \leqslant 1$ g m$^{-3})$ and some cloud occurrences. Note, in particular, the peaks around 12:00 UTC (6th and 7th February) and those on 8th February. However, there are sometimes some relatively short delays (at most one hour) between the predictions of the model and the radar observations. Differences may be explained by the fact that the weather conditions at the Maïdo are complex, especially due to the topography. Also, the reflectivity threshold of −15 dBZ is a mean value with a certain degree of arbitrariness. The transition between what is cloud and what is drizzle (or light rain) is rather fuzzy and occurs around this reflectivity. What is sure is that cloud droplet reflectivity is very low (and negative). If we had chosen a lower reflectivity threshold to identify cloud droplets and then calculate L_c as per the above equation, the number of black dots in Fig. 3 would have been smaller. However, the results obtained from the three equations that define the model provide a relatively reasonable estimate of cloud creation/dissipation.

3.2. Comparison with microwave radiometric measurements

3.2.1. Pristine oceanic context: Saint Denis

Fig. 4 shows a simulation of 72 h between the 1st February 2019 (00:00 UTC) and the 3th February 2019 (23:59 UTC). For this case study representative of a pristine oceanic context, the measurements of L_v and N_0 presented in the previous section (Fig. 1B) have been implemented in the model as input data. Based on independent observations, a relative humidity threshold of 80% has been chosen for the binary value of α.

The top graph represents the evolution of L_c, L_r, N_d and L_v, the middle graph shows the variation of $L_{c,d}, L_l$ and N_a, and the bottom graph is an estimation of the cloud albedo (R_c) and the Cloud Optical Thickness (COT). The increasing of L_c is concomitant to a decreasing of N_d, *i.e.* bigger droplets are numerous. This was not so apparent for the above case study (Maïdo). The reason may be that, now, the values of N_d, like those of N_0, are relatively small (pristine environment), so that any change is quite easy to see. In addition, each increase of L_c is followed by the activation of rain (L_r increases) about 10 min later. The typical evolution of L_c is characterized by some peaks at around 1 g m^{-3} in a

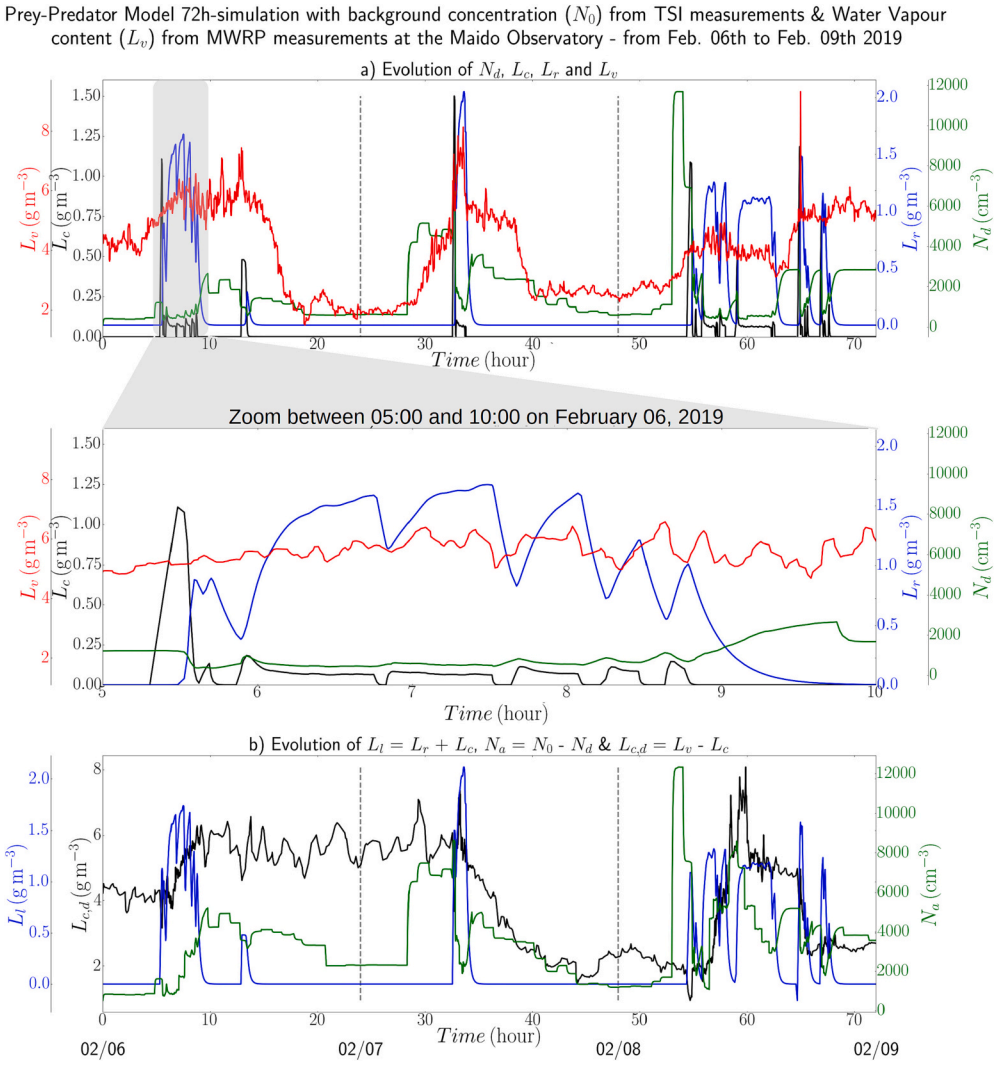

Fig. 2. Maïdo Observatory (z = 1 km above ground level), from the 6th to the 8th February 2019: evolution of (a) L_c, L_r, N_d, L_v and of (b) $L_{c,d}, L_l$ and N_a for a simulation of 72 h with background concentration from TSI measurements and water vapour from the MWRP measurements.

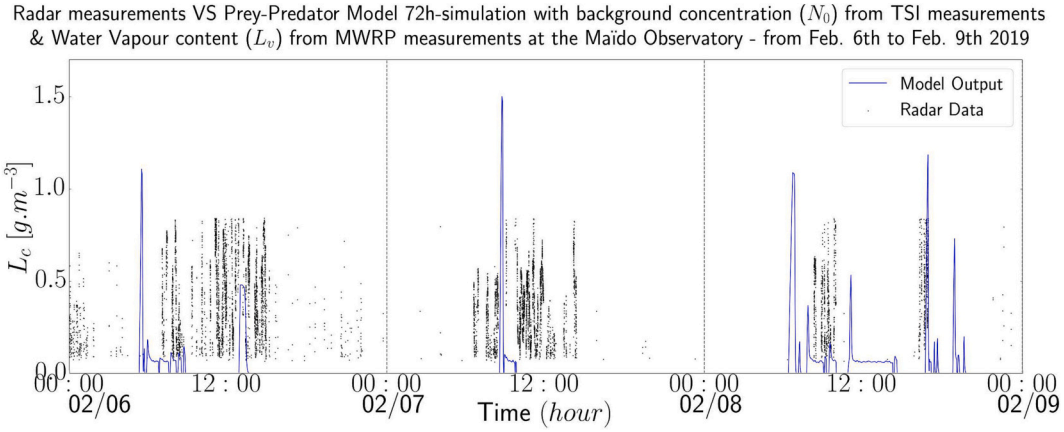

Fig. 3. Evolution of L_c from radar measurements (in black) and model (Eq. (2)) predictions (in blue) for a simulation of 72 h with a background concentration and a water vapour content measured, resp., by the CPC TSI and the MWRP at the Maïdo Observatory, between the 6th and 8th February 2019 (as for Fig. 2).

"background" of $L_c \leqslant 0.25$ g m^{-3}. The maximum of the rain water content is approximately 5 g m^{-3}. The second graph indicates that the amount of water available in the system $L_{c,d}$ follows the behaviour (in time and in order of magnitude) of the absolute humidity L_v. This can be explained by the fact that water vapour content is, in this Tropical marine area, almost constant and much greater (≈ 8 g m^{-3}) than the cloud water content, so that changes in L_c (and even sporadic peaks) do not substantially impact L_v (and so $L_{c,d}$). The same occurs for N_a which

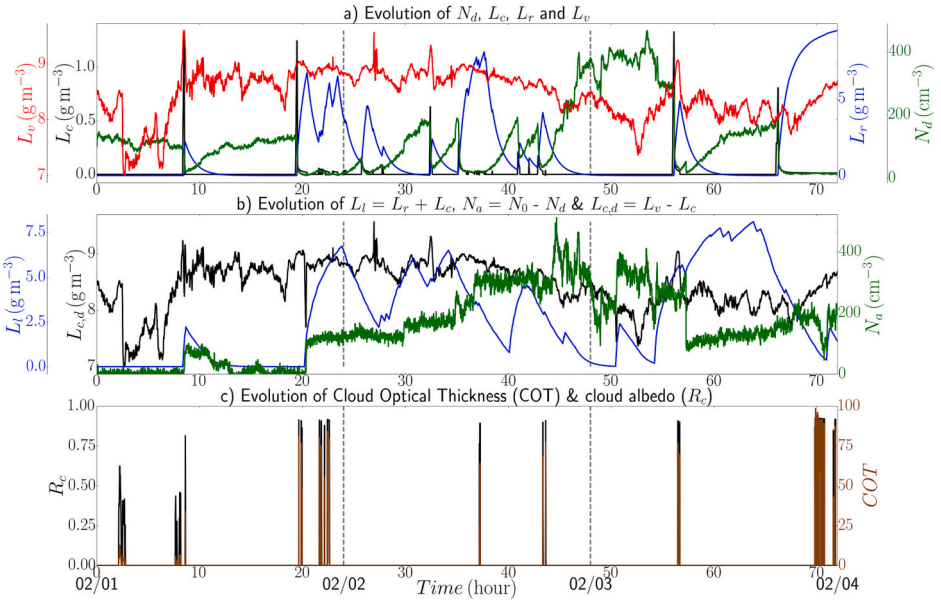

Fig. 4. Saint Denis (Reunion Island), between 1st and 4th February 2019: evolution of (a) L_c, L_r, N_d and L_v, (b) $L_{c,d}, L_l$ and N_a, and, (c) Cloud Optical Thickness (COT) and albedo (R_c), with background aerosol concentration (N_0) from TSI measurements and water vapour content (L_v) from MWRP measurements.

presents an evolution and orders of magnitude similar to N_0, except at the end of the simulation, despite of the changes in N_d. This means that, as for water vapour, the system is fed with a substantial flux of aerosol that permits to compensate possible modifications due to the evolution of N_d. This is quite interesting knowing the pristine marine conditions. Finally, concerning the cloud optical properties, the estimated COT is mainly greater than 75 and the $R_c > 0.75$. This corresponds to low altitude marine clouds of the stratus type, which is consistent with the kind of clouds usually present in this region.

The modeled cloud water content is now compared with the cloud water content determined from radiometric measurements (Fig. 5). It is observed that the general behavior of cloud formation is well represented by our system of three equations. Indeed, putting aside four point clouds during this simulation of 72 h, the model correctly reproduces the appearance and dissipation of clouds, although some delays of at most one hour are not rare. Moreover, the orders of magnitude of the modeled cloud water content are consistent with those furnished by the MWRP. It has to be recalled that the MWRP does not measure directly cloud water content but derives it from an internal algorithm based on adiabaticity of cloud formation. Another explanation of the observed differences may be that the input data (L_v and N_0) are not colocated. During AEROMARINE, the MWRP was deployed in Saint Denis (north of Reunion Island) while aerosol concentrations were measured during light flights to the west off the Island. However, the global agreement between our model and the MWRP outputs is not so bad, which suggests that the results presented herein are consistent.

3.2.2. Urban context: Lille

We now turn to an urban context and run the model for a 72 h-simulation between the 10th October 2020 (00:00 UTC) and the 12th October 2020 (23:59 UTC) using, as input data, measurements (L_v, N_0) from the ATOLL station.Here too, based on independent observations, a relative humidity threshold of 80% has been chosen for the determination of α.

Fig. 6 displays the outputs out the model. The response of the Prey-Predator model (Eq. (2)) is presented in Fig. 6 as previously. It can be seen clouds appear (L_c first peak) about 12:00 after the beginning to the simulation, when the water vapour content L_v is high enough ($L_v \geqslant 2.5$ g m^{-3}). Here too, the equations being based on the species competition approach, cloud formation leads to rain formation with a time delay of about 15 min, a typical value for the triggering of rain (Rogers and Yau, 1996). Rain is then followed by cloud dissipation. It can also be seen that the amount of rain depends on the amount of absolute humidity, *i.e.* the larger L_v, the greater L_r.

Fig. 6b indicates that $L_{c,d}$ evolves as L_v with the same orders of magnitude (between 2 and at most 10 g m^{-3}). The amount of aerosols (N_a) remaining in the system is of the same order of magnitude as N_d. Finally, the amount of liquid water (L_l) is maximum when there is formation of clouds and rain over a sufficiently long time (see, *e.g.*, during the second day of the simulation).

With respect to the estimated COT and R_c (Fig. 6c), it can be noted that the simulated COT varies between 0 and 100. Given the altitude considered ($z = 2$ km), it can be deduced that we are in presence of

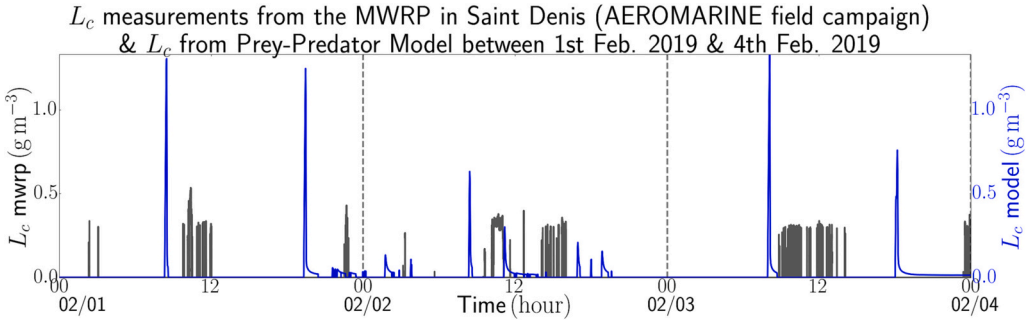

Fig. 5. Same as Fig. 4 but comparing $L_c(t)$ between radiometric measurements and the model.

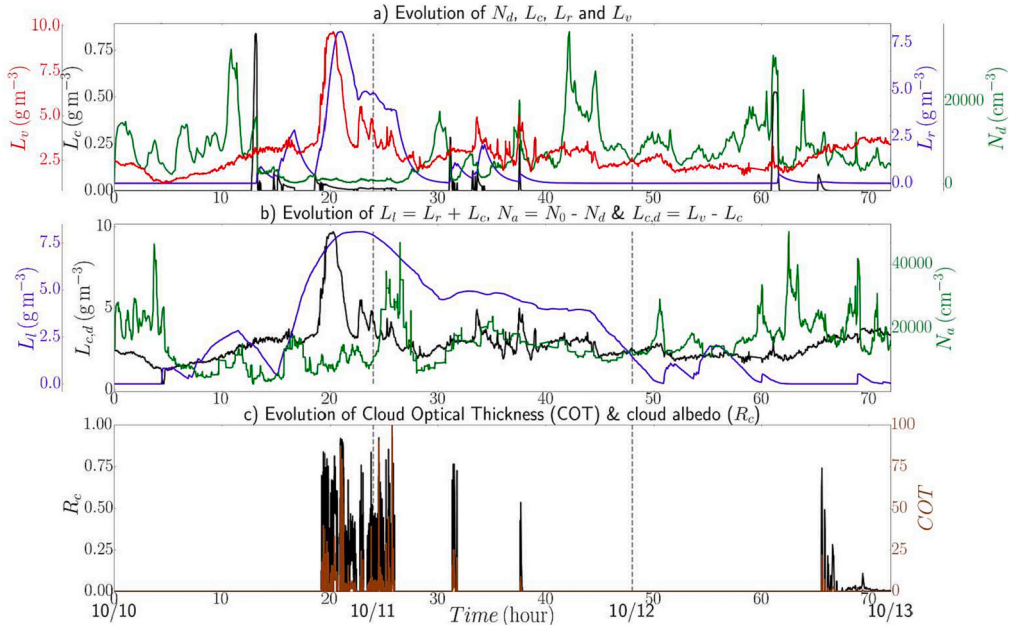

Fig. 6. Lille, between the 10th and 12th October 2020: evolution of (a) L_c, L_r, N_d and L_v, (b) $L_{c,d}, N_a$ and L_l, and, (c) Cloud Optical Thickness (COT) and albedo (R_c) for a simulation of 72 h, with aerosol concentration and water vapour content from the ATOLL station.

cumulus ($COT \leqslant 5$), stratocumulus ($5 < COT < 25$) and stratus ($COT \geqslant 25$) (Rossow and Schiffer, 1991; Hahn et al., 2001). In this simulation of 72 h, the stratus is dominant. Similarly, the calculated R_c is essentially between 0.25 and 0.75, which supports the hypothesis that the simulated clouds are of the stratus type (Stephens and Webster, 1981).

Comparing the modeled L_c with the L_c measured by the MWRP (Fig. 7), a good agreement between the model and the *in situ* measurements is observed in terms of the presence/absence of clouds. In addition, when there is a cloud, the model gives orders of magnitude similar to those of the MWRP. However, generally speaking, the model underestimates the values of the cloud water content. A bias in the model cannot be excluded, of course, but, as already mentioned, a possible explanation is also the way the MWRP calculates the cloud water content (see above).

In addition, we find that our model is as close as possible to *in situ* measurements in the continental context in Lille, *i.e.* with higher aerosol concentrations.

3.3. Other simulations

Similar simulations have been performed with other independent dates for the same situations considered above. Results (not shown) exhibit similar behaviour as those obtained: the model gives realistic orders of magnitude of the different macroscopic variables, cloud and rain formations are delayed by about 20 min, model and observation agree about the cloud occurrences and magnitudes of the cloud water content. We can thus be conclude that the model proposes a good evaluation of the macroscopic and essential behaviour of a cloud system, especially regarding the water vapour, aerosol, cloud and rain interaction.

3.4. Adaptation to a two-dimensional grid

The model being fast (simulation time around 10 s for a simulation over 72 h and showing quite good behaviors for aerosol-water vapour-cloud-rain interactions, it seems interesting to compare its outputs with those of more complete two-dimensional (2D) models. Herein, comparisons have been performed with the ERA5 reanalysis (5th generation of European Centre for Medium-Range Weather Forecasts - ECMWF - reanalysis for the global climate and weather). They combine model outputs with observations into a globally complete and consistent dataset (ECMWF, 2016). In particular, ERA5 provides hourly estimates for absolute and relative humidities, as well as cloud water content, at different levels of pressure. We have chosen the level 900 hPa, *i.e.* $z \approx 1$ km asl (available online),[6] and the data have been regridded on a regular 0.25° latitude-longitude grid. This data of humidity allows to feed the model in terms of L_v. To compare the prediction of our model with the ERA5 reanalysis requires to assume that each pixel (0.25°) of the whole grid is described by Eq. (2). In other words, keeping in mind that Eq. (2) describe the behaviour of a cloud as a bulk, it is assumed that, for an area of p pixels, there are p independent Eq. (2), each of them predicting an evolution of L_c in a given pixel. There is no coupling between the pixels. The model presented in this work is thus adapted to a 2D grid in this sense.

Here, the comparison with ERA5 is presented for simulations over seven days for the two following concrete case studies:

1. in a continental context, over the Hauts-de-France region centered around Lille, in the box [49.5°N-51.5°N; 2°E-4°E], from the 1st to the 7th October 2020.
2. in an oceanic context around Reunion Island, in the box [20°S-21°S; 54°E-55°E], from the 9th to the 15th February 2019.

It is worth precising that, in the absence of other data, we use ERA5 to get humidity data which serve as an input parameter to feed hourly the model. The model does not calculate humidity, because L_v is not, here, a degree of freedom (there is no differential equation for L_v). Hence, humidity is not calculated and, *a fortiori*, not compared nor updated (or corrected) under the basis of some model-ERA5 comparisons. As we will see hereafter, the only comparison concerns liquid water content L_c. In this sense, the model is not constrained since there is no need to revise the simulation as the model is running.

[6] This altitude is typical of marine low-level clouds (see *e.g.* Bony et al., 2000; Sèze and Pawlowska, 2001). In addition, the first levels of ERA5 are 1000, 900, 800 hPa ($z \approx 0, 1, 2$ km). An altitude of 1 km seems thus reasonable to test the abilities of the model.

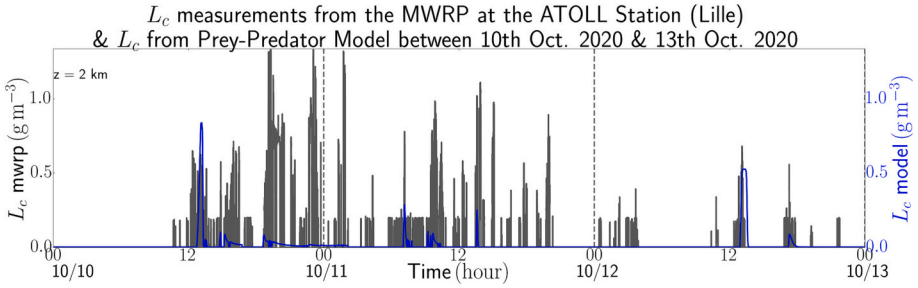

Fig. 7. Same as Fig. 6 but comparing $L_c(t)$ between radiometric measurements and the model.

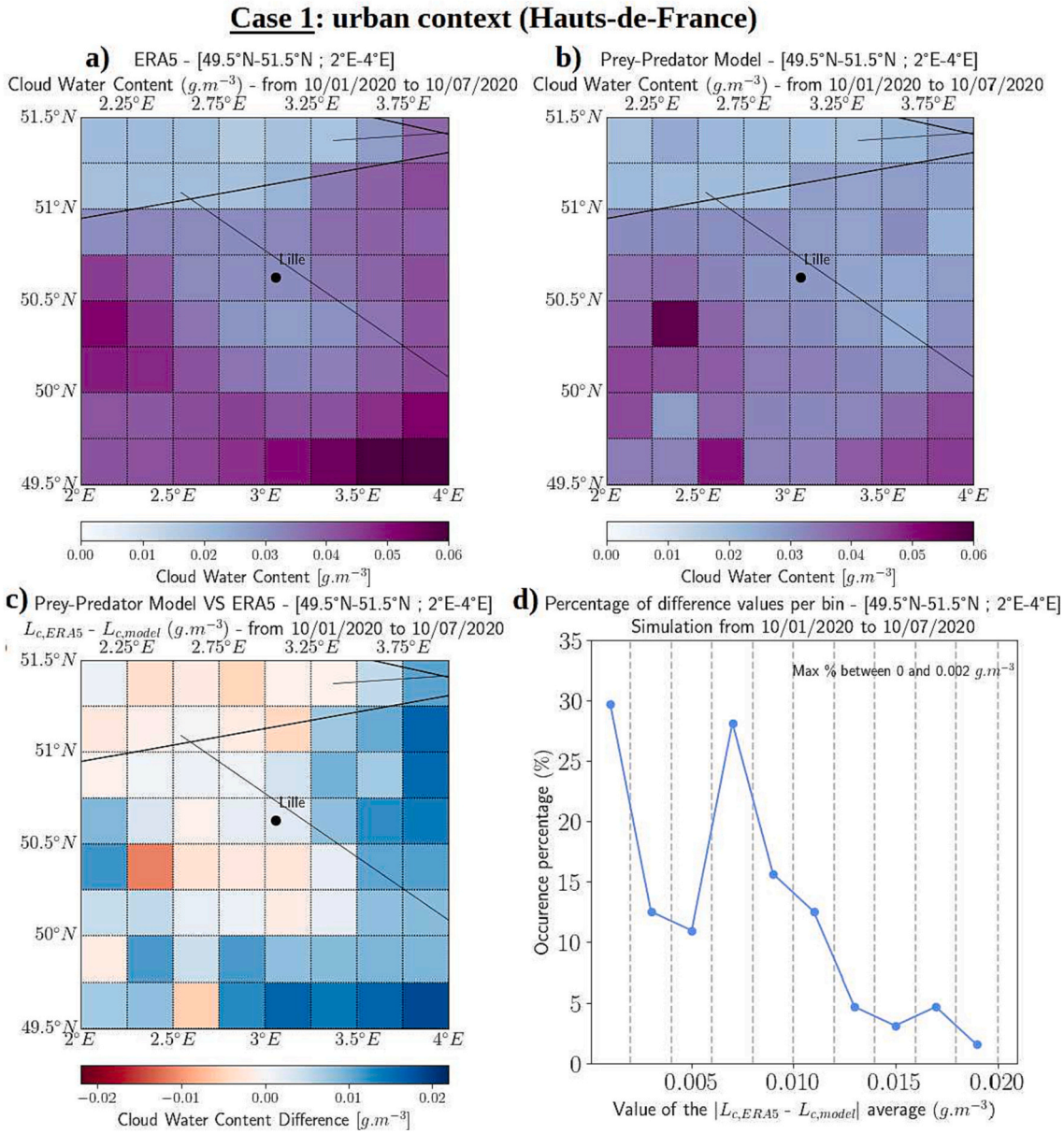

Fig. 8. Average of the cloud water content (L_c in g m^{-3}) from ERA5 (a), from our model (b), average of $L_{c,ERA5}$ - $L_{c,Model}$ difference (c) obtained from a 7-days simulation of the model over the Hauts-de-France region, between the 1st and 7th of October 2020. Panel (d) is the probability density function of $L_{c,ERA5}$ - $L_{c,Model}$.

3.4.1. *Case 1: urban context (Hauts-de-France)*

Fig. 8 displays the cloud water content averaged over the whole simulations (7 days) given by the ERA5 reanalysis (a) and computed by our model (b); the difference is displayed on the panel (c). Clearly, the ERA5 and the modeled cloud fields behave consistently since both give, on average, a cloud water content below 0.06 g m^{-3} and similar spatial distribution of clouds around Lille. There are more clouds on the South-West and on the South of Lille than on the North and North-East. The

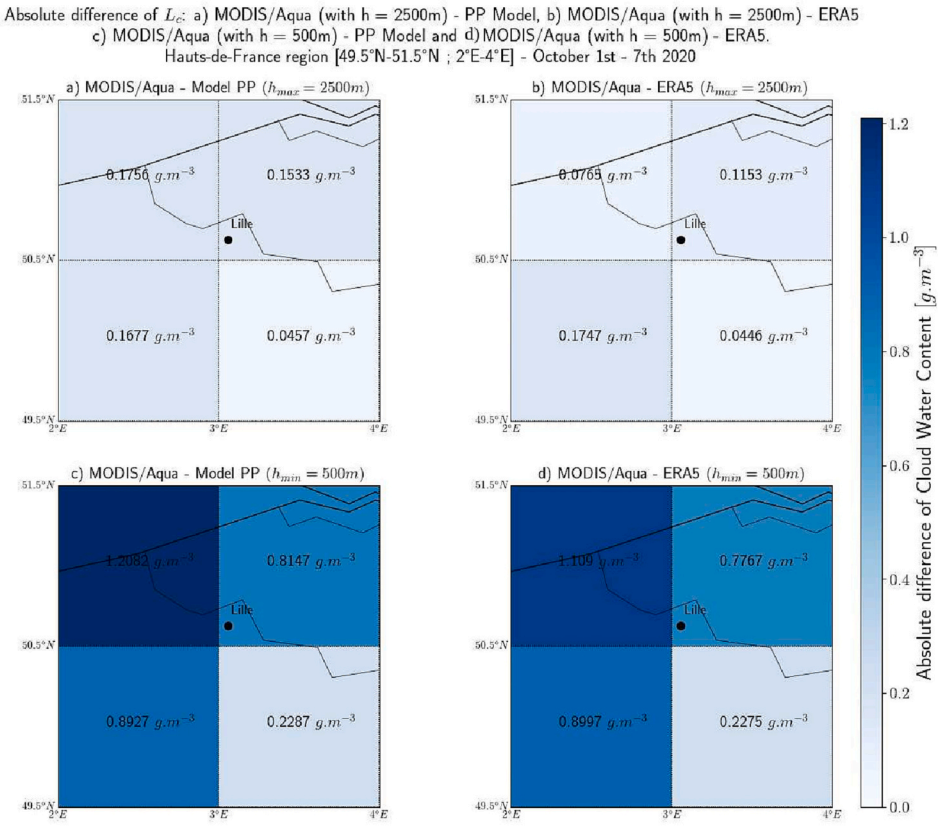

Fig. 9. Top: Comparison of the L_c-differences (averaged over seven days, 1st-7th October 2020) between AQUA, the model, and ERA5. On the left: difference between AQUA and the model. On the right: difference between AQUA and ERA5. A minimum and a maximum cloud depths of 500 m (panels on the bottom) and 2500 m (panels on the top) have been assumed. Calculations have been performed by distinguishing four quadrants (North-East, North-West, South-West, South-East). Bottom: Scatterplots of the absolute differences per quadrant. The tilted dashed line is the 1 : 1 line.

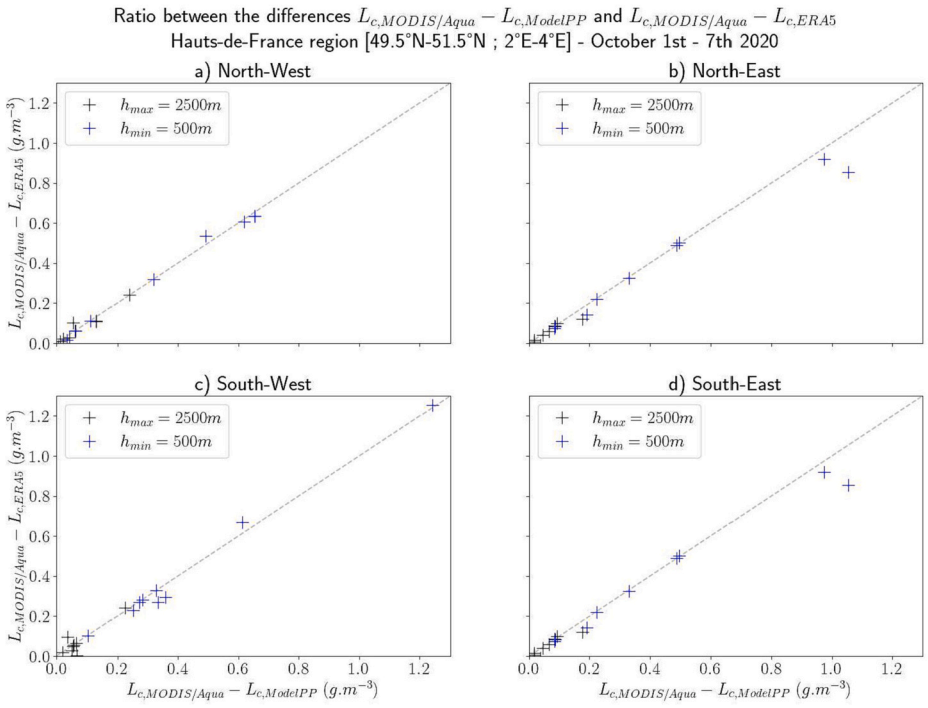

difference between the two mean fields of L_c is particularly interesting: it never exceeds 0.02 g m^{-3} and, in a great part of the area considered, this difference is even close to zero. The probability density function of the difference is displayed on Fig. 8d; it shows that the discrepancies between ERA5 and our model is smaller than 0.01 g m^{-3} with a peak of 30% below 0.002 g m^{-3} and another one at about 0.007 g m^{-3}.

The comparison with the liquid products of the satellite MODIS/AQUA over the seven days considered is also interesting. In particular AQUA provides the liquid water path which can be compared with the cloud water content (L_c) given by ERA5 and by the model if one assumes a cloud

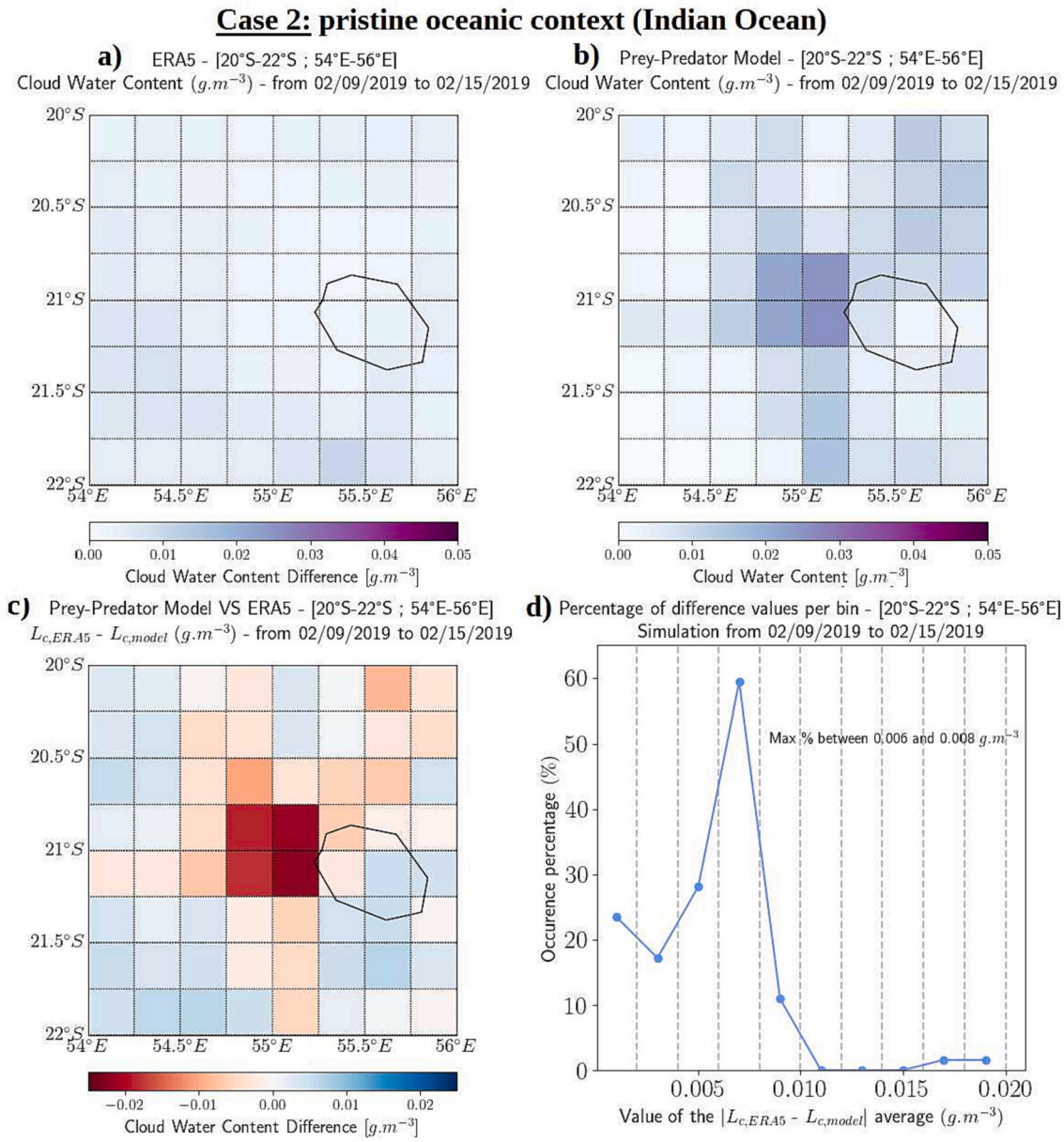

Fig. 10. Same as Fig. 8 but in the oceanic context around Reunion Island and between 9th and 15th February of 2019.

depth. Fig. 9 displays the average (over the seven days) difference in cloud water content, between AQUA and the model on one hand and, between AQUA and ERA5 on the other hand, assuming two cloud depths, $h_{min} = 500$ m and $h_{max} = 2500$ m. We have distinguished four quadrants (North-East, North-West, South-West and South-East). It can be seen, in particular, that the differences between AQUA and the model are almost the same than the differences between AQUA and ERA5, which means that the model (Eq. (2)) behaves as well as ERA5. This is corroborated by the scatterplots on the bottom of the Figure obtained by considering the differences each day (not an average).

3.4.2. *Case 2: pristine oceanic context (Indian Ocean)*

Fig. 10 is the same as Fig. 8 but for the second case considered (oceanic context, around Reunion Island). The same comments as just above can be done: on average over the seven days of simulations, (1) the ERA5 cloud water content (Fig. 10a) and and the cloud water content given by our model (Fig. 10b) agree quite well; (2) the difference between these cloud water contents is lower than 0.02 g m^{-3} with a probability density function of the difference values analogous to that of Fig. 10d which peaks at 60% for a difference between 0.006 and 0.008 g m^{-3}. Note that the values between 0.01 and 0.02 g m^{-3} are, for this case, much less represented. It can be noted that the most important differences are on the West of Reunion Island, with an underestimation of L_c by our model, *i.e.* where the AEROMARINE field campaign and so where the airborne aerosol measurements took place (Mascaut et al., 2022). Since the aerosol concentrations were measured in the free troposphere, and not from the surface, they may be underestimated and so not exactly representative of the background concentrations of the marine aerosols around Reunion Island.

As above, a comparison with the liquid products of the satellite MODIS/AQUA have been performed (Fig. 11). The results are better than for the Lille-case since the differences in L_c with AQUA are much smaller for both the model and ERA5. Again, these differences are almost the same, meaning that the model is, in this sense, equivalent to ERA5. The scatterplots on the bottom of the Figure confirm this conclusion.

For the case of Reunion Island, satellite images from SEVIRI/MSG were exploitable. Fig. 12 displays some SEVIRI/MSG satellite images corresponding to the considered area. Some specific days have been chosen,

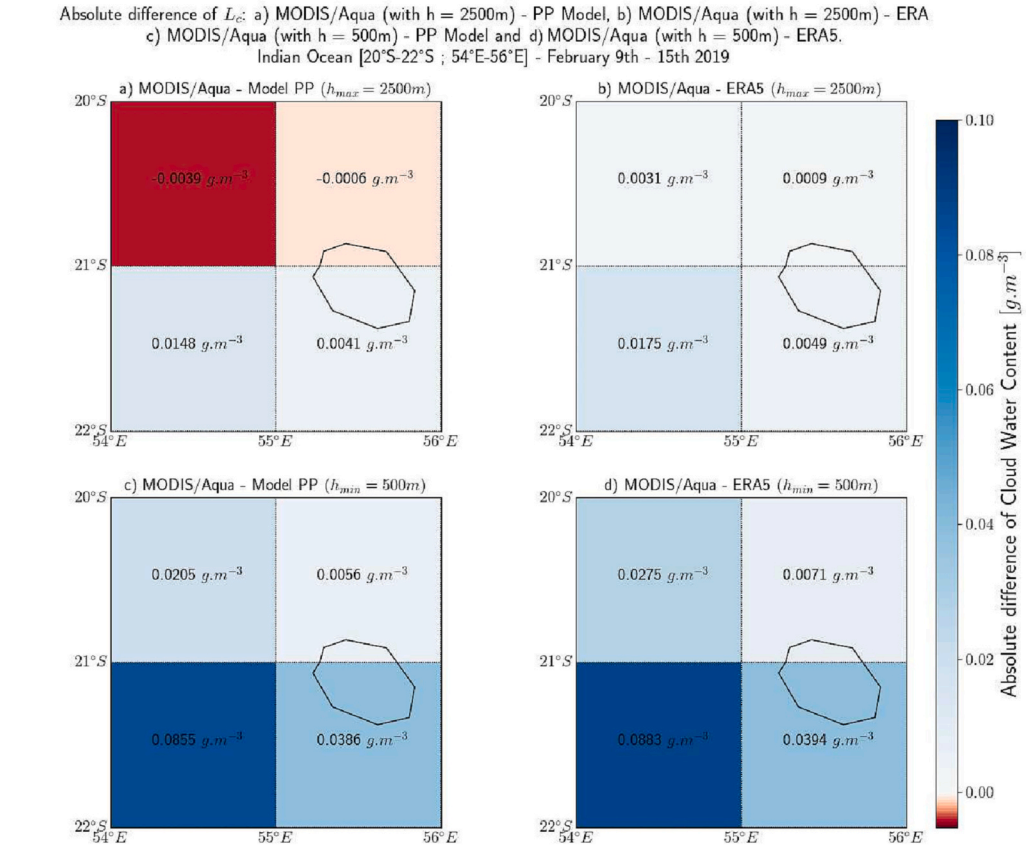

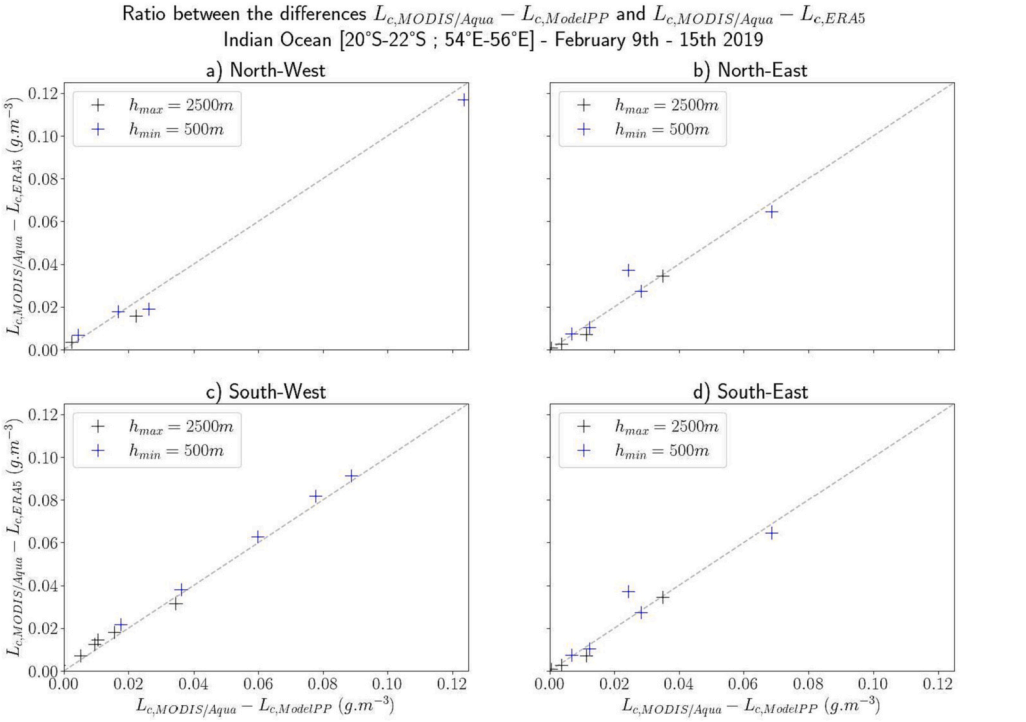

Fig. 11. Same as Fig. 9 but around Reunion Island.

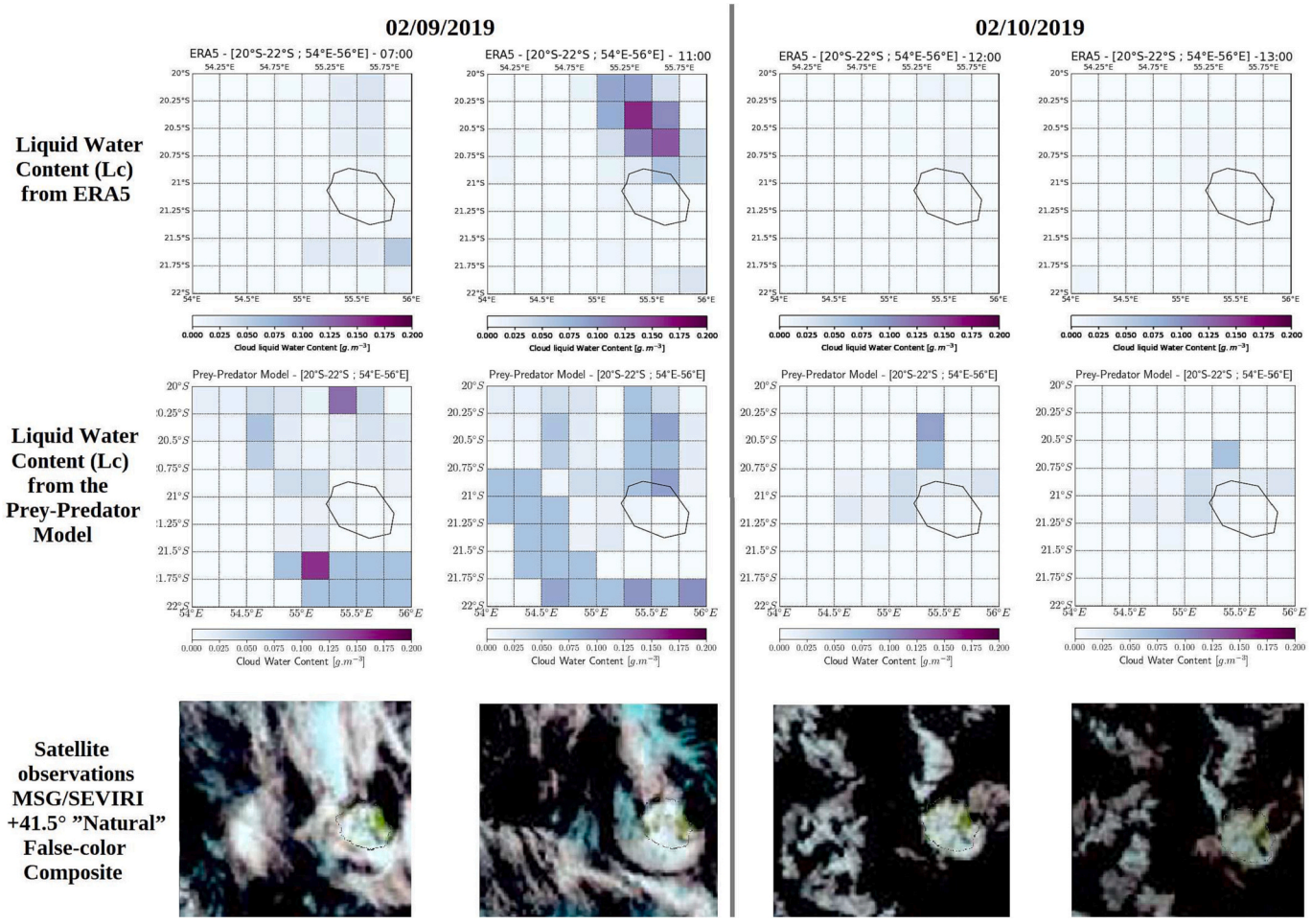

Fig. 12. Qualitative comparison with SEVIRI/MSG satellite images for some specific days over Reunion Island.

which permit to explain particularly the L_c differences on the West of Reunion Island. It can indeed be observed that our model is closer to satellite observations than the ERA5 reanalysis which do not "see" the clouds West of the island. In addition, our model seem to predict more cloud occurrences than ERA5, in agreement with what the satellite images indicate. For the other days that cover this simulation of seven days, our model, ERA5 and the satellite images agree together (not shown).

4. Conclusion

In this study, we have proposed a nonlinear bulk model which is able to describe the physics of a water vapour-aerosol-cloud–rain system. The model is inspired by models of species competition dynamics. It consists in a set of three nonlinear coupled differential equations which generalizes the previous model of Pujol and Jensen (2019) by considering explicitly the water vapour content as an independent variable of the system. The presentation of such a model has been motivated by the need to associate idealized models with few degrees of freedom, which captures the essential physics, with exhaustive models which represent, as completely as possible, all the complex cloud dynamics.

The effectiveness of the system of equations proposed in capturing the important macro physics of cloud behaviour has been tested for three concrete cases:

- in a pristine oceanic region (Saint-Denis, Reunion Island), in an aerosol background close to the pre-industrial conditions with relatively stable thermodynamic conditions,
- at the high-altitude Maïdo Observatory (2.2 km of altitude asl, Reunion Island), with a well marked diurnal/nocturnal cycle of the thermodynamics and aerosol content of the troposphere.
- in the urban context of Lille (Région Hauts-de-France), which is characterized by relativity varying humidity and aerosol contents, as revealed in the measurements from the ATOLL platform.

For each of these regions, the kinetic constants of the set of equations have been optimized, for the three situations just mentioned, by combining a Monte Carlo approach and least-squares minimization. The method we have chosen for this affords the possibility to use the model for determining kinetic constants that otherwise are only available from non-simple theoretical considerations or otherwise *ad hoc* empirical fitting.

Compared with real observations (radar and radiometric measurements), the results obtained show that the model reproduces efficiently the macro behavior of clouds: cloud occurrences (formation/dissipation), orders of magnitude of the cloud water content, cloud and rain content links are well captured by our model. A possible explanation of the discrepancies that can exist between the model and the observations (*e.g.* short delays in cloud occurrence, small differences in L_c values) is that instruments which furnish the input data are not always collocated in spacetime (*e.g.* in the case of the AEROMARINE field campaign).

The time step of the numerical solver is around 0.1 s minimum. In addition, it has a relatively short calculation time (lower than 10 s for a 72 h simulation). Because of this, we have then used the model within a two-dimensional (2D) horizontal grid and compared the results with the ERA5 reanalyses in two situations: a continental context above the Région

Hauts-de-France on one hand, and in the South-West Indian Ocean (around Reunion Island) on the other hand.

Simulations for seven days have been performed for these two cases. Once again, our model shows promising results for the horizontal organization of cloud fields, since the system of three equations provides results close to those obtained by complete reanalysis. For the whole 2D grids considered, the difference between the reanalysed cloud water content (ERA5) and the computed cloud water content (our set of equations) never exceeds 0.02 g m^{-3}; the most probable difference is rather close to 0.007 g m^{-3}. The spatiotemporal resolution of our model is, of course, adaptable depending on the user needs; it can be used in any region and at the desired altitude provided that the environmental humidity and aerosol concentrations be available. Comparisons with satellite observations, when exploitable, namely with MODIS/AQUA liquid products, show that the model behaves as well as ERA5 since both exhibit similar differences with AQUA in terms of liquid water content. In addition, from the qualitative comparisons with the geostationary images of SEVIRI/MSG over the Southern Indian Ocean, around Reunion Island, one sees that, sometimes, the model predictions are better than those of ERA5 in the sense that this last one seems to not see cloudy pixels. The model presented here appears thus to present reasonable and physically realistic results in terms of cloud behaviour, comparable to other models. We mention that detailed 2*D* fields of humidity and aerosols over a large area in the Indian Ocean would be welcome for the present model.

The promising results of this model of water Vapour-Aerosol-Cloud Interactions (VACI) suggest some perspectives. We indicate some of them. First, machine learning and/or artificial intelligence could be useful in the optimization of the kinetic constants according to the situation considered (continental, maritime, etc.). A further step would be to determine the terms which describe the relevant physical processes involved in VACI by an artificial intelligence. This perspective should pave the way to new ways of analyzing and modeling cloud physics. Another way to improve our system of equations would be to consider other characteristics, such as radiation for example, and to examine how it is impacted by some properties of the clouds like precipitation. With respect to this, we should likely have to introduce explicitly the number of raindrop (N_r) as a degree of freedom. In the present version of the model, it has not been considered in order to retain some measure of simplicity and because focus has been put first on the cloud component (in general $N_d \gg N_r$). A third point is the introduction of a coupling between systems as modeled by Eq. (2). For instance, in the comparison with ERA5 reanalyses, each pixel of the grid was assumed to be an independent system of Eq. (2). Pixel interactions are lacking in order to investigate more deeply cloud field organization. Different approaches can be envisioned, but they can be classified into two categories: (1) those of deterministic essence, which would consist, for instance, to consider *N* sets of Eq. (2) (one per pixel) and to add a coupling term between them that could depend on wind; (2) those of stochastic (or statistical) nature, which could be inspired for example from the 2D Ising model in magnetism. This last avenue is currently under investigation and will be presented in a future paper.

CRediT authorship contribution statement

Faustine Mascaut: Conceptualization, Methodology, Investigation, Writing – original draft, Writing – review & editing, Software. **Olivier Pujol:** Conceptualization, Methodology, Investigation, Software, Supervision, Writing - original draft, Writing - review & editing. **Jérôme Brioude:** Investigation, Resources, Supervision, Writing - original draft, Writing - review & editing. **Andrew Jensen:** Conceptualization, Writing - review & editing. **Marc Lefranc:** Formal analysis, Methodology. **Stéphanie Evan:** Resources. **Suzanne Crumeyrolle:** Resources.

Data availability

Data will be made available on request.

Acknowledgements

We are grateful to the Labex CAPPA (ANR-11-LABX-0005–01) which has funded this work in the context of the Cloud-aerosol interactions work package. We acknowledge the ECMWF for providing freely reanalysis. The authors thank the French national LEFE/INSU program which financed the AEROMARINE field campaign as well as the CONCIRTO project (ANR-17-CE01-0005–01). The authors thanks the Principal Investigator, Karine Sellegri, (k.sellegri@opgc.univ-bpclermont.fr) of the particle counter (CPC TSI) located at the Maïdo Observatory, for providing freely datasets.

References

Baray, J.L., Courcoux, Y., Keckhut, P., Portafaix, T., Tulet, P., Cammas, J.P., Hauchecorne, A., Godin-Beekmann, S., De Mazière, M., Hermans, C., Desmet, F., Sellegri, K., Colomb, A., Ramonet, M., Sciare, J., Vuillemin, C., Hoareau, C., Dionisi, D., Duflot, V., Vérèmes, H., Porteneuve, J., Gabarrot, F., Gaudo, T., Metzger, J.M., Payen, G., Leclair De Bellevue, J., Barthe, C., Posny, F., Abchiche, A., Delmas, R., Ricaud, P., 2013. Maïdo observatory: a new high-altitude station facility at Reunion Island (21 S, 55 E) for long-term atmospheric remote sensing and in situ measurements. Atmos. Meas. Tech. 6, 2865–2877. https://doi.org/10.5194/amt-6-2865-2013.

Bellouin, N., Quaas, J., Gryspeerdt, E., Kinne, S., Stier, P., Watson-Parris, D., Boucher, O., Carslaw, K.S., Christensen, M., Daniau, A.L., Dufresne, J.L., Feingold, G., Fiedler, S., Forster, P., Gettelman, A., Haywood, J.M., Lohmann, U., Malavelle, F., Mauritsen, T., McCoy, D.T., Myhre, G., Mülmenstädt, J., Neubauer, D., Possner, A., Rugenstein, M., Sato, Y., Schulz, M., Schwartz, S.E., Sourdeval, O., Storelvmo, T., Toll, V., Winker, D., Stevens, B., 2020. Bounding global aerosol radiative forcing of climate change. Rev. Geophys. 58, e2019RG000660 https://doi.org/10.1029/2019RG000660. URL:https://agupubs.onlinelibrary.wiley.com/doi/abs/10.1029/2019RG000660.

Bony, S., Collins, W.D., Fillmore, D.W., 2000. Indian ocean low clouds during the winter monsoon. J. Clim. 13, 2028–2043. https://doi.org/10.1175/1520-0442(2000)013<2028:IOLCDT>2.0.CO;2. URL:https://journals.ametsoc.org/view/journals/clim/13/12/1520-0442_2000_013_2028_iolcdt_2.0.co_2.xml.

Bovchaliuk, V., Goloub, P., Podvin, T., Veselovskii, I., Tanre, D., Chaikovsky, A., Dubovik, O., Mortier, A., Lopatin, A., Korenskiy, M., Victori, S., 2016. Comparison of aerosol properties retrieved using garrlic, liric, and raman algorithms applied to multi-wavelength lidar and sun/sky-photometer data. Atmos. Meas. Tech. 9, 3391–3405. https://doi.org/10.5194/amt-9-3391-2016. URL:https://amt.copernicus.org/articles/9/3391/2016/.

Chen, G., Canonaco, F., Tobler, A., Aas, W., Alastuey, A., Allan, J., Atabakhsh, S., Aurela, M., Baltensperger, U., Bougiatioti, A., De Brito, J.F., Ceburnis, D., Chazeau, B., Chebaicheb, H., Daellenbach, K.R., Ehn, M., El Haddad, I., Eleftheriadis, K., Favez, O., Flentje, H., Font, A., Fossum, K., Freney, E., Gini, M., Green, D.C., Heikkinen, L., Herrmann, H., Kalogridis, A.C., Keernik, H., Lhotka, R., Lin, C., Lunder, C., Maasikmets, M., Manousakas, M.I., Marchand, N., Marin, C., Marmureanu, L., Mihalopoulos, N., Močnik, G., Ne˛cki, J., O'Dowd, C., Ovadnevaite, J., Peter, T., Petit, J.E., Pikridas, M., Matthew Platt, S., Pokorná, P., Poulain, L., Priestman, M., Riffault, V., Rinaldi, M., Różański, K., Schwarz, J., Sciare, J., Simon, L., Skiba, A., Slowik, J.G., Sosedova, Y., Stavroulas, I., Styszko, K., Teinemaa, E., Timonen, H., Tremper, A., Vasilescu, J., Via, M., Vodička, P., Wiedensohler, A., Zografou, O., Cruz Minguillón, M., Prévôt, A.S., 2000. European aerosol phenomenology 8: Harmonised source apportionment of organic aerosol using 22 year-long acsm/ams datasets. Environ. Int. 166, 107325 https://doi.org/10.1016/j.envint.2022.107325. URL:https://www.sciencedirect.com/science/article/pii/S0160412022002525.

Douville, H., K.Raghavan, Renwick, J., Allan, R., Arias, P., Barlow, M., Cerezo-Mota, R., Cherchi, A., Gan, T., Gergis, J., Jiang, D., Khan, A., Mba, W.P., Rosenfeld, D., Tierney, J., Zolina, O., 2021. Water cycle changes. in climate change 2021: The physical science basis. In: Masson-Delmotte, V., Zhai, P., Pirani, A., Connors, S.L., Péan, C., Berger, S., Caud, N., Chen, Y., Goldfarb, L., Gomis, M.I., Huang, M., Leitzell, K., Lonnoy, E., Matthews, J.B.R., Maycock, T.K., Waterfield, T., Yelekçi, O., Yu, R., Zhou, B. (Eds.). Contribution of Working Group I to the Sixth Assessment Report of the Intergovernmental Panel on Climate Change. doi:10.1017/9781009157896.010.

ECMWF, 2016. IFS Documentation CY43R1 - Part IV: Physical Processes. Number 4 in IFS Documentation, ECMWF. URL:https://www.ecmwf.int/node/17117, doi:10.21957/sqvo5yxja.

Foucart, B., Sellegri, K., Tulet, P., Rose, C., Metzger, J.M., Picard, D., 2018. High occurrence of new particle formation events at the maïdo high-altitude observatory (2150 m), réunion (Indian Ocean). Atmos. Chem. Phys. 18, 9243–9261. https://doi.org/10.5194/acp-18-9243-2018. URL:https://acp.copernicus.org/articles/18/9243/2018/.

Francis, D., Chaboureau, J.P., Nelli, N., Cuesta, J., Alshamsi, N., Temimi, M., Pauluis, O., Xue, L., 2021. Summertime dust storms over the arabian peninsula and impacts on radiation, circulation, cloud development and rain. Atmos. Res. 250, 105364.

https://doi.org/10.1016/j.atmosres.2020.105364. URL:https://www.sciencedirect.com/science/article/pii/S0169809520313016.
Gryspeerdt, E., Goren, T., Smith, T.W.P., 2021. Observing the timescales of aerosol–cloud interactions in snapshot satellite images. Atmos. Chem. Phys. 21, 6093–6109. https://doi.org/10.5194/acp-21-6093-2021. URL:https://acp.copernicus.org/articles/21/6093/2021/.
Guilpart, E., Vimeux, F., Evan, S., Brioude, J., Metzger, J.M., Barthe, C., Risi, C., Cattani, O., 2017. The isotopic composition of near-surface water vapor at the maïdo observatory (reunion island, southwestern indian ocean) documents the controls of the humidity of the subtropical troposphere. J. Geophys. Res.: Atmos. 122, 9628–9650. https://doi.org/10.1002/2017JD026791.
Hahn, C.J., Rossow, W.B., Warren, S.G., 2001. Isccp cloud properties associated with standard cloud types identified in individual surface observations. J. Clim. 14, 11–28. https://doi.org/10.1175/1520-0442(2001)014<0011:ICPAWS>2.0.CO;2. URL:https://journals.ametsoc.org/view/journals/clim/14/1/1520-0442_2001_014_0011_icpaws_2.0.co_2.xml.
Hänggi, P., Talkner, P., Borkovec, M., 1990. Reaction-rate theory: fifty years after kramers. Rev. Mod. Phys. 62, 251–341. https://doi.org/10.1103/RevModPhys.62.251. URL:https://link.aps.org/doi/10.1103/RevModPhys.62.251.
Held, I.M., 2005. The gap between simulation and understanding in climate modeling. Bull. Am. Meteorol. Soc. 86, 1609–1614. URL:http://www.jstor.org/stable/26221382.
Karstens, U., Simmer, C., Ruprecht, E., 1994. Remote sensing of cloud liquid water. Meteorol. Atmos. Phys. 54, 157–171. https://doi.org/10.1007/BF01030057.
Koren, I., Wang, C., 2008. Cloud–rain interactions: as complex as it gets. Environ. Res. 3, 045018 https://doi.org/10.1088/1748-9326/3/4/045018.
Laj, P., Bigi, A., Rose, C., Andrews, E., Lund Myhre, C., Collaud Coen, M., Lin, Y., Wiedensohler, A., Schulz, M., Ogren, J.A., Fiebig, M., Gliß, J., Mortier, A., Pandolfi, M., Petäja, T., Kim, S.W., Aas, W., Putaud, J.P., Mayol-Bracero, O., Keywood, M., Labrador, L., Aalto, P., Ahlberg, E., Alados Arboledas, L., Alastuey, A., Andrade, M., Artíñano, B., Ausmeel, S., Arsov, T., Asmi, E., Backman, J., Baltensperger, U., Bastian, S., Bath, O., Beukes, J.P., Brem, B.T., Bukowiecki, N., Conil, S., Couret, C., Day, D., Dayantolis, W., Degorska, A., Eleftheriadis, K., Fetfatzis, P., Favez, O., Flentje, H., Gini, M.I., Gregorič, A., Gysel-Beer, M., Hallar, A. G., Hand, J., Hoffer, A., Hueglin, C., Hooda, R.K., Hyvärinen, A., Kalapov, I., Kalivitis, N., Kasper-Giebl, A., Kim, J.E., Kouvarakis, G., Kranjc, I., Krejci, R., Kulmala, M., Labuschagne, C., Lee, H.J., 2020. A global analysis of climate-relevant aerosol properties retrieved from the network of global atmosphere watch (gaw) near-surface observatories. Atmos. Meas. Tech. 13, 4353–4392. https://doi.org/10.5194/amt-13-4353-2020. URL:https://amt.copernicus.org/articles/13/4353/2020/.
Long, A.B., 1974. Solutions to the droplet collection equation for polynomial kernels. J. Atmos. Sci. 31, 1040–1052. https://doi.org/10.1175/1520-0469(1974)031<1040:STTDCE>2.0.CO;2. URL:https://journals.ametsoc.org/view/journals/atsc/31/4/1520-0469_1974_031_1040_sttdce_2_0_co_2.xml.
Louf, V., Pujol, O., Sauvageot, H., Riédi, J., 2015. Seasonal and diurnal water vapour distribution in the sahelian area from microwave radiometric profiling observations. Q. J. R. Meteorol. Soc. 141, 2643–2653. https://doi.org/10.1002/qj.2550.
Mallet, P.E., Pujol, O., Brioude, J., Evan, S., Jensen, A., 2018. Marine aerosol distribution and variability over the pristine southern indian ocean. Atmos. Environ. 182, 17–30. https://doi.org/10.1016/j.atmosenv.2018.03.016.
Mascaut, F., Pujol, O., Verreyken, B., Peroni, R., Metzger, J.M., Blarel, L., Podvin, T., Goloub, P., Sellegri, K., Thornberry, T., Duflot, V., Tulet, P., Brioude, J., 2022. Aerosol characterization in an oceanic context around reunion island (aeromarine field campaign). Atmos. Environ. 118770 https://doi.org/10.1016/j.atmosenv.2021.118770.
Mortier, A., Goloub, P., Podvin, T., Deroo, C., Chaikovsky, A., Ajtai, N., Blarel, L., Tanre, D., Derimian, Y., 2013. Detection and characterization of volcanic ash plumes over lille during the eyjafjallajökull eruption. Atmos. Chem. Phys. 13, 3705–3720. https://doi.org/10.5194/acp-13-3705-2013. URL:https://acp.copernicus.org/articles/13/3705/2013/.
Pruppacher, H., Klett, J., 2010. Microstructure of atmospheric clouds and precipitation. In: Microphysics of Clouds and Precipitation. Springer, Netherlands, pp. 10–73. https://doi.org/10.1007/978-0-306-48100-0_2.
Pujol, O., Jensen, A., 2019. Cloud–rain predator–prey interactions: Analyzing some properties of the koren–feingold model and introduction of a new species-competition bulk system with a hopf bifurcation. Phys. D 399, 86–94. https://doi.org/10.1016/j.physd.2019.04.007. URL:https://www.sciencedirect.com/science/article/pii/S0167278918301520.
Rogers, R.R., Yau, M.K., 1996. A short course in cloud physics. Elsevier.
Rosenfeld, D., Sherwood, S., Wood, R., Donner, L., 2014. Climate effects of aerosol-cloud interactions. Science (Am. Assoc. Adv. Sci.) 343, 379–380.
Rossow, W.B., Schiffer, R.A., 1991. Isccp cloud data products. Bull. Am. Meteorol. Soc. 72, 2–20. https://doi.org/10.1175/1520-0477(1991)072<0002. URL:https://journals.ametsoc.org/view/journals/bams/72/1/1520-0477_1991_072_0002_icdp_2_0_co_2.xml.
Sauvageot, H., 1992. Radar Meteorology.
Sauvageot, H., Omar, J., 1987. Radar reflectivity of cumulus clouds. J. Atmos. Ocean. Technol. 4, 264–272. https://doi.org/10.1175/1520-0426(1987)004<0264:RROCC>2.0.CO;2. URL:https://journals.ametsoc.org/view/journals/atot/4/2/1520-0426_1987_004_0264_rrocc_2_0_co_2.xml.
Seifert, A., Beheng, K.D., 2001. A double-moment parameterization for simulating autoconversion, accretion and selfcollection. Atmos. Res. 265–281. https://doi.org/10.1016/S0169-8095(01)00126-0. URL:http://www.sciencedirect.com/science/article/pii/S0169809501001260. 13th International Conference on Clouds and Precipitation.
Seinfeld, J., Pandis, S., 1998. Atmospheric Chemistry and Physics: From Air Pollution to Climate Change. URL:https://www.bibsonomy.org/bibtex/2c037a32c1277cdaba937076d8eff1109/gsmith.
Seinfeld, J.H., Bretherton, C., Carslaw, K.S., Coe, H., DeMott, P.J., Dunlea, E.J., Feingold, G., Ghan, S., Guenther, A.B., Kahn, R., Kraucunas, I., Kreidenweis, S.M., Molina, M.J., Nenes, A., Penner, J.E., Prather, K.A., Ramanathan, V., Ramaswamy, V., Rasch, P.J., Ravishankara, A.R., Rosenfeld, D., Stephens, G., Wood, R., 2016. Improving our fundamental understanding of the role of aerosol–cloud interactions in the climate system. Proc. Nat. Acad. Sci. 113, 5781–5790. https://doi.org/10.1073/pnas.1514043113. URL:https://www.pnas.org/doi/abs/10.1073/pnas.1514043113, arXiv:https://www.pnas.org/doi/pdf/10.1073/pnas.1514043113.
Simu, S.A., Miyazaki, Y., Tachibana, E., Finkenzeller, H., Brioude, J., Colomb, A., Magand, O., Verreyken, B., Evan, S., Volkamer, R., Stavrakou, T., 2021. Origin of water-soluble organic aerosols at the maïdo high-altitude observatory, réunion island, in the tropical Indian Ocean. Atmos. Chem. Phys. 21, 17017–17029. https://doi.org/10.5194/acp-21-17017-2021. URL:https://acp.copernicus.org/articles/21/17017/2021/.
Stathopoulos, S., Tsonis, A.A., Kourtidis, K., 2021. On the cause-and-effect relations between aerosols, water vapor, and clouds over East Asia. Theoret. Appl. Climatol. 144, 711–722. https://doi.org/10.1007/s00704-021-03563-7.
Stephens, G.L., Webster, P.J., 1981. Clouds and climate: sensitivity of simple systems. J. Atmos. Sci. 38, 235–247. https://doi.org/10.1175/1520-0469(1981)038<0235:CACSOS>2.0.CO;2. URL:https://journals.ametsoc.org/view/journals/atsc/38/2/1520-0469_1981_038_0235_cacsos_2_0_co_2.xml.
Stevens, B., Bony, S., Brogniez, H., Hentgen, L., Hohenegger, C., Kiemle, C., L'Ecuyer, T. S., Naumann, A.K., Schulz, H., Siebesma, P.A., Vial, J., Winker, D.M., Zuidema, P., 2020. Sugar, gravel, fish and flowers: Mesoscale cloud patterns in the trade winds. Q. J. R. Meteorol. Soc. 146, 141–152. https://doi.org/10.1002/qj.3662. URL:https://rmets.onlinelibrary.wiley.com/doi/abs/10.1002/qj.3662, arXiv:https://rmets.onlinelibrary.wiley.com/doi/pdf/10.1002/qj.3662.
Sèze, G., Pawlowska, H., 2001. Cloud cover analysis with meteosat-5 during indoex. J. Geophys. Res.: Atmos. 106, 28415–28426. https://doi.org/10.1029/2001JD900097. URL:https://agupubs.onlinelibrary.wiley.com/doi/abs/10.1029/2001JD900097.
Villani, P., Picard, D., Marchand*, N., Laj, P., 2007. Design and validation of a 6-volatility tandem differential mobility analyzer (vtdma). Aerosol Sci. Technol. 41, 898–906. https://doi.org/10.1080/02786820701534593.
Weston, M.J., Temimi, M., Nelli, N.R., Fonseca, R.M., Thota, M.S., Valappil, V.K., 2021. On the analysis of the low-level double temperature inversion over the united arab emirates: A case study during April 2019. IEEE Geosci. Remote Sens. Lett. 18, 346–350. https://doi.org/10.1109/LGRS.2020.2972597.
Wettlaufer, J.S., 2016. Editorial: Climate science: An invitation for physicists. Phys. Rev. Lett. 116, 150002 https://doi.org/10.1103/PhysRevLett.116.150002. URL:https://link.aps.org/doi/10.1103/PhysRevLett.116.150002.
Xu, W., Ovadnevaite, J., Fossum, K.N., Lin, C., Huang, R.J., Ceburnis, D., O'Dowd, C., 2022. Sea spray as an obscured source for marine cloud nuclei. Nat. Geosci. 15, 282–286. https://doi.org/10.1038/s41561-022-00917-2.
Yousef, L.A., Temimi, M., Molini, A., Weston, M., Wehbe, Y., Mandous, A.A., 2020. Cloud cover over the arabian peninsula from global remote sensing and reanalysis products. Atmos. Res. 238, 104866 https://doi.org/10.1016/j.atmosres.2020.104866. URL:https://www.sciencedirect.com/science/article/pii/S0169809519301218.
Zhu, J., Che, H., Xia, X., Yu, X., Wang, J., 2019. Analysis of water vapor effects on aerosol properties and direct radiative forcing in China. Sci. Total Environ. 650, 257–266. https://doi.org/10.1016/j.scitotenv.2018.09.022. URL:https://www.sciencedirect.com/science/article/pii/S0048969718334405.